CrossMark

Assessment of the Indian summer monsoon in the WRF regional climate model

**Attada Raju · Anant Parekh · J. S. Chowdary ·
C. Gnanaseelan**

Abstract The performance of the regional climate model, Weather Research and Forecasting in simulating the three dimensional moist and thermodynamic structure of Indian summer monsoon (ISM) during 2001–2011 is examined in this study. The model could simulate monsoon elements and convective precipitation zones over ISM region with some overestimation. Statistical analysis of sub-regional precipitation indicates that model has better skill over the monsoon core region with correlation of 0.7 and root mean square error of 2.3 mm day^{-1} with respect to observations. The model simulated seasonal mean vertical structures of temperature and water vapour mixing ratio (WVMR) are consistent with the Atmospheric Infrared Sounder observations. However, the core of low level jet is shifted southward in the model due to unrealistic convective heating over the lower latitudes of Indian Ocean and southern peninsular India. The tropical easterly jet is confined to 15°N in the model, which is due to the mid-tropospheric cold bias over the Tibetan region. The meridional asymmetric bias of sea level pressure (SLP) in model leads to weaker vertical wind shear, limiting the northward migration of maximum rain band to south of 23°N. These discrepancies have marked effects on the proper simulation of monsoon climate. The large scale spatial patterns of SLP, precipitation and winds during active and break spells are well simulated by the model. The lead-lag evolution of vertical structure of model temperature shows baroclinic structure during the active phase. It is evident from the observations that enhanced (suppressed) convection is generally preceded by a low-level moist (dry) anomaly and followed by a low-level dry (moist) anomaly. The model is inadequately representing the temporal evolution of vertical moist and thermodynamic processes. The evolution of vertical structures of temperature and WVMR is better simulated in the break phase compared to that of active phase. The evolution of cyclonic vorticity in the model is different from the observations during the convective phase. In short the model has limitations in representing convectively unstable regimes. It is anticipated that these findings will significantly contribute to the regional climate model assessment programs.

1 Introduction

The Indian Summer Monsoon (ISM) is considered as an atmospheric response to seasonal changes in land–sea thermal contrast, induced by the annual cycle of the solar zenith angle (e.g., Meehl 1994; Webster et al. 1998; Wu et al. 2012). ISM rainfall (ISMR) is important due to its impact on agrarian economies of countries like India (e.g., Gadgil 1996). The country receives more than 80 % of the annual rainfall during a short span of 4 months from June to September (e.g., Rajeevan et al. 2013). Kripalani et al. (2007) studied the ability of global climate models (GCMs) in simulating the ISMR and its variability and found several discrepancies in the simulation of regional precipitation. According to Krishna Kumar et al. (2005) GCM applications in the ISM region are limited by an insufficient representation of orography due to their coarse grid resolution. This advocates the use of finer resolution regional climate

A. Raju (✉) · A. Parekh · J. S. Chowdary · C. Gnanaseelan
Indian Institute of Tropical Meteorology, Dr. Homi Bhabha Road,
Pashan, Pune 411 008, Maharashtra, India
e-mail: rajua@tropmet.res.in

🖄 Springer

models (RCMs). A number of attempts have been made in the past to demonstrate the capability of RCMs to simulate the ISM features (Bhaskaran et al. 1996; Jacob and Podzum 1997; Vernekar and Ji 1999; Lee and Suh 2000; Bhaskar Rao et al. 2004; Dobler and Ahrens 2010; Mukhopadhyay et al. 2010; Hariprasad et al. 2011; Lucas-Picher et al. 2011; Saeed et al. 2012; Srinivas et al. 2012; Raju et al. 2014a, 2014b).

Above studies indicate that the RCMs can simulate mean monsoon features and its variability to a greater extent. However, significant improvement in the simulation of ISMR climatology in RCMs is crucial for making any further progress towards seasonal prediction (Feng and Fu 2006; Lucas-Picher et al. 2011). Mukhopadhyay et al. (2010) discussed the thermodynamic structure of the simulated monsoon climate and brought out the strengths and weaknesses of different convective closures. Nie et al. (2010) suggested that the dynamic and thermodynamic assessment may be appropriate for monsoons. When simulating a thermally direct monsoon circulation, one might ask whether the observed thermodynamic structure of monsoon is reproduced in the model well (Boos and Hurley 2013). John and Soden (2007) showed the importance of temperature and water vapor biases in global climate models. Raju et al. (2014a) reported considerable uncertainties encountered in the vertical structures of moist thermodynamics during ISM-2010 in Weather Research and Forecasting (WRF) model. There are many RCM studies (e.g. Mukhopadhyay et al. 2010; Srinivas et al. 2012) for simulation of ISM but their domain is confined to a smaller region, which is expected to be more constrained by the driving fields and has less freedom to evolve the dynamic features. Recently, several studies (e.g. Lucas-Picher et al. 2011) suggested that large domains should be used in regional climate simulations to allow the atmospheric circulation to get modified by the RCM on spatial scales that are not well represented by the GCM. The model fidelity might also improve with the domain size as the boundary forcing is away from the core region of interest and also allows the development of its internal dynamics, mesoscale and large scale systems of monsoon on its own in the regional models (e.g. Wang et al. 2004; Lucas-Picher et al. 2011; Bhaskaran et al. 2012; Diaconescu and Laprise 2013). Apart from this, coordinated efforts involving several programs have led to the generation of an increasing amount of regional climate simulations over South Asian region. For instance, Coordinated Regional Climate Downscaling Experiment (CORDEX) under World Climate Research Program is coordinating a range of RCM simulations forced by reanalysis data, and also by 20th century GCM runs to provide a benchmark framework for model evaluation and its application for climate implication studies over the south Asian domain. Hence the assessment of

the model with large domain is important for such applications. It is also important to note that none of the previous studies evaluated the model vertical moist thermodynamic structures with satellite observations due to the unavailability of observations.

The uniqueness of this paper from the previous studies is that the chosen study area covers the entire monsoon domain and it evaluates the vertical moist and thermodynamic structure with the observations. Such validation for dynamic and thermodynamic structure of the simulated monsoon climate in the regional models brings out the strengths and weaknesses of convective closures. In this context the present paper identifies and quantifies the merits and demerits in the horizontal and vertical structure of ISM and its active and break phases in WRF model over the monsoon core region (MCR; 69°E to 88°E and 18°N to 28°N), where ISMR plays crucial role (Rajeevan et al. 2010) in terms of mean monsoon as well as intraseasonal scales. An assessment of the salient features of mean ISM and an evaluation of vertical moist and thermodynamic structures for seasonal mean and ISO time scales are the primary objectives of the study. The paper is constructed as follows. Section 2 provides a brief description of the model, data used and methodology. Section 3 briefly presents the model simulated mean ISM features and seasonal evolution of rainfall over MCR. The vertical structures of dynamic and thermodynamic components associated with ISM over MCR are described in Sect. 4. Assessment of mean monsoon ISO features simulated by the model is discussed in Sect. 5. Section 6 presents summary and discussion.

2 Model details, data used and methodology

2.1 Model details

The model used here is the Advanced Research WRF model (Skamarock et al. 2008). It is a limited area, non-hydrostatic primitive equation model with multiple options for various physical parameterization schemes. The time split integration uses a third order Runge–Kutta scheme with smaller time step for acoustic and gravity wave modes. The physical options used in this study consist of the Purdue Lin (Chen and Sun 2002) scheme for microphysics, the convective parameterization scheme of Betts and Miller (1986) but modified further by Janjic (1994) as Betts-Miller-Janjic (BMJ) for subscale precipitation as it produced a reasonable ISM climatology in WRF (Mukhopadhyay et al. 2010). The Rapid Radiative Transfer Model (Mlawer et al. 1997) and Dudhia scheme (Dudhia 1989) are used for long wave and shortwave radiation respectively, Monin–Obukhov (Monin and Obukhov 1954) similarity scheme for surface layer and the Yonsei University planetary boundary layer scheme

for boundary layer (Noh et al. 2003) are used. The model domain extends between 30°E to 175°E zonally and 30°S to 40°N meridionally, which covers the extent of the monsoon domain (Ramage 1971) consisting of 370 by 198 grid points with 45 km grid spacing. The model resolution (45 km) considered in this study is in line with the model resolution used by CORDEX regional climate simulations and this spatial resolution is adequate to resolve the hydrology-related processes for seasonal scale simulations (e.g. Dobler and Ahrens 2010; Srinivas et al. 2012) and sufficient enough to capture the relevant synoptic scale phenomena governing the climate over ISM region. Thus this study explores ISM simulation using a well tested suite of parameterization schemes for the entire monsoon domain. The model has 40 vertical levels with the top of the model at 10 hPa. The model has been integrated starting from 1 May to 1 October for every year during 2001–2011. National Centers for Environmental Prediction (NCEP) final analysis data (FNL) on $1° \times 1°$ spatial resolution at every 6 h interval is used for the initial and boundary conditions. The simulation corresponding to June to September (JJAS) is used in the present study allowing 1 month (May) as a spin up time. One month spin up time is sufficient for the dynamical equilibrium between the lateral forcing and the internal physical dynamics of the model (Anthes et al. 1989). The daily real time global Sea Surface Temperature (SST) product (Thiebaux et al. 2003) is used as the slowly varying lower boundary condition for the model. Topography as well as snow cover information are obtained from United States Geological Survey. The model output is retrieved at daily interval corresponding to 00 UTC.

2.2 Data used and methodology

The European Center for Medium-Range Weather Forecasts (ECMWF) Interim reanalysis (here after ERAI) data available (Simmons et al. 2007) at a spectral resolution of T255, which is approximately $0.7° \times 0.7°$ (re-gridded to $1° \times 1°$) is used to compare the model simulated (re-gridded to $1° \times 1°$) mean fields during 2001–2011. The model simulated fields are also compared with parent analysis, which is NCEP FNL. The daily precipitation simulated by the model (re-gridded to $1° \times 1°$ resolution) is compared with the daily gridded rainfall data made available by India Meteorological Department (IMD) over India at the same resolution (Rajeevan et al. 2006), the Global Precipitation Climatology Project (GPCP) rainfall data (Huffman et al. 2001) available at $1° \times 1°$ and Tropical Rainfall Measuring Mission (TRMM) daily precipitation (3B42V6; Huffman et al. 2007) data available at $0.25° \times 0.25°$ (re-gridded to $1° \times 1°$) over the study area. The re-gridding is done using a bilinear interpolation technique. Here, the unknown value is determined considering the closest 2×2 neighbourhood

of known grid point values, surrounding the unknown computed location. It is important to mention that many studies have followed this procedure for such comparison (e.g. Mukhopadhyay et al. 2010; Taraphdar et al. 2010; Dobler and Ahrens 2010).

The evolution of vertical moist and thermodynamic structures of the model is compared with Atmospheric Infrared Sounder (AIRS) and ERAI data. The AIRS data has a horizontal resolution of $1° \times 1°$ and 24 pressure levels from 1,000 to 1 hPa for temperature and 12 pressure levels from 1,000 to 100 hPa for specific humidity. AIRS is the most advanced temperature and humidity sounding system ever deployed (Parkinson 2003). AIRS data provides global 3-dimensional distributions of moisture and temperature with very high spatial–temporal resolutions (Fu et al. 2006; John and Soden 2007; Tian et al. 2010; Wong et al. 2011). The details of AIRS observations are described by Aumann et al. (2003). AIRS WVMR profiles have uncertainties of 10–30 % and biases of a few percent in 2 km layers for all non-polar conditions and temperature uncertainty is about 1 K in the first 1 km (e.g. Divakarla et al. 2006). Since AIRS makes tropical measurements around 0130 and 1330 local time, the daily averaged temperature and WVMR at each location are actually the averages of the two measurements. These temperature and WVMR profiles (Level-3) from June to September during 2003–2011 are used in this study. These state of the art data sets have provided an opportunity to diagnose monsoon moist and thermodynamic features. However model monsoon dynamic features are compared with the ERAI reanalysis product.

The large (spatial) scale comparative assessment of model simulated mean fields with the observations/reanalysis fields is carried out using pattern correlation (PC) over the whole domain (20°S to 40°N and 30°E to 175°E). Further, threat score (TS) is estimated for rainfall, which is a metric to measure the model ability of categorical rainfall forecast (Anthes et al. 1989). It is also known as the critical success index (CSI, Schaefer 1990). These scores are computed based on the contingency table as given in Table 1. The formula for computing TS is

$$TS = \frac{A}{A + B + C} \tag{1}$$

Table 1 Contingency table for TS

Given categories	Observed	
Model	Yes	No
Yes	Hits (A)	False alarms (B)
No	Misses (C)	Correct negatives (D)

The A, B, C and D are represent the number of occurrences for which model precipitation or observed precipitation did (yes) or did not (no) reach or exceed a given threshold

A, B and C are hits, false alarms and misses respectively. For a perfect forecast, TS is 1 whereas TS is zero for the worst forecast. TS analysis is performed for simulated seasonal rainfall over MCR under three different categories, low (<5 mm day^{-1}), moderate ($5-10$ mm day^{-1}), and high (≥ 10 mm day^{-1}). The selection of these categories based on daily mean rainfall and its standard deviation over MCR (e.g. Goswami et al. 2006). Active and break phases of ISM in the observations and model are identified as per the criteria proposed by Rajeevan et al. (2010). Area averaged daily rainfall anomaly over MCR is normalized by its daily standard deviation, whenever the normalized rainfall is more (less) than $+1.0$ (-1.0) consecutively for three days or more, it is considered as active (break) period. The active and break days are (identified based on precipitation index) representative measure of monsoon activity during the season (Rajeevan et al. 2006, 2010). The lead lag composites of the active (break) phases are prepared by fixing the lag zero as the central day of the active (break) spells for further analysis.

3 Fundamental features of ISM

This section briefly describes the large scale features of ISM. The ISM is characterized by land-sea thermal contrast, which implies a steep sea level pressure (SLP) gradient between northern India and southern Indian Ocean. Figure 1 depicts the spatial distribution of monthly mean SLP and midtropospheric temperature from model (a–d), ERAI (e–h) and their differences (i–l). Model shows reasonable skill in reproducing the SLP gradient, location of surface heat low over northwest India and the position of the monsoon trough (Fig. 1a–d). However, negative (positive) SLP bias over the southwestern part of India (northwest Pacific region) is reported from June to September. These zonal biases in the model might have strong impact on the monsoon circulation and precipitation. The model SLP bias has latitudinal asymmetry centered at 10°N (i.e., northern part has positive bias and southern part has negative bias) throughout the season. This asymmetry in the bias indicates that model has weak meridional SLP gradient due to weak land-sea thermal contrast. The analysis reveals that model could simulate the major features of SLP distribution associated with ISM albeit with some biases over specific regions. The PC of SLP distribution between model and ERAI indicates that the discrepancies in SLP increase with the progression of season (Table 2). Midtropospheric temperature is strongly associated with convection and precipitation during ISM. The model is able to simulate the mean spatial distribution of midtropospheric temperature as in ERAI. Maximum meridional temperature gradient during the peak monsoon months (July, August) is captured by the model (Fig. 1b, c).

Model has cold bias (~ -2 K) over the Tibetan region and warm bias over Indian land mass (~ 1 K) as well as over northwest Pacific (1–3 K) throughout the season.

The most important dynamical feature of ISM is the formation of low level jet (LLJ) over the Arabian Sea (AS). Figure 2 illustrates the monthly mean low level (850 hPa) wind fields from model (Fig. 2a–d), ERAI (Fig. 2e–h) and the corresponding wind biases (Fig. 2i–l). The model could simulate the low level monsoon circulation with the PC of 0.66, 0.64, 0.49, and 0.43 respectively during June to September. The mean monsoon flow in model strengthens during peak monsoon months over the western AS and is in agreement with ERAI, but LLJ is slightly broader than ERAI. It is important to note that the model simulated wind fields show a well-defined cyclonic circulation over the monsoon trough region. The core of LLJ is shifted southeastward, which is due to the strong convective heating (positive bias of 1–2 K) at low latitudes in the model (Fig. 1). According to Joseph and Sijikumar (2004) the axis of LLJ is oriented southeastward when the convective heating of the atmosphere is over the low latitudes of Indian Ocean. On the other hand, westward shift of model LLJ is due to the unrealistic distribution of SLP. The easterly (westerly) bias over the western Pacific to MCR (east coast of Africa) is mainly due to the unrealistic zonal pressure gradient in the model (Fig. 1). Thus analysis reveals that the circulation discrepancies enhance with the progression of monsoon season.

Upper tropospheric (200 hPa) winds during ISM are mainly characterized by the Tropical Easterly Jet (TEJ) and Tibetan anticyclone during the monsoon (Krishnamurti and Bhalme 1976). Figure 3 depicts the monthly mean upper tropospheric winds from the model (a–d), ERAI (e–h) and their differences (i–l). Model could simulate upper tropospheric circulation features such as Tibetan anticyclone, TEJ and subtropical westerly jet in agreement with ERAI. However, Tibetan anticyclonic circulation in the model is located in the east of its normal position (Fig. 3i). During the peak monsoon, TEJ is weaker than observed in the model and its northward extension is confined to 15°N, whereas it is extended up to 25°N in ERAI. The northward shift of westerlies is realistically simulated by the model but the corresponding north south orientation of TEJ is not simulated by the model. The model has very strong westerly bias over the Indian land mass and western Pacific region. Location of Tibetan anticyclone associated with ISM is slightly shifted to south (Fig. 3a–d). Strong cold bias over the Tibetan plateau in the model at midtroposphere, representing weak heating explains the weaker TEJ than observed, resulting its confinement to south of 15 ºN (Krishnamurti and Bhalme 1976).

In order to identify the improvement in regional fine scale features associated to ISM with respected to parent
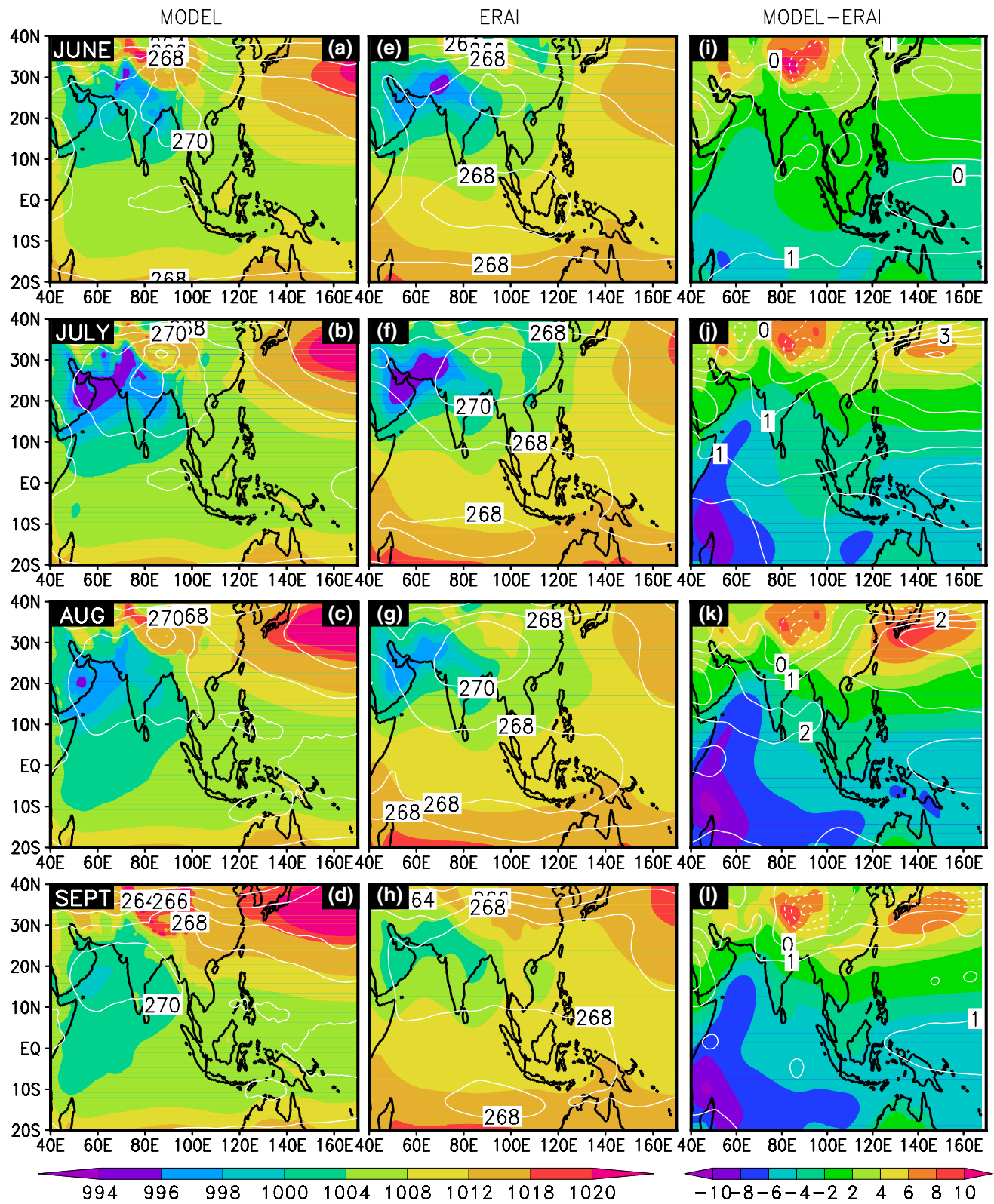
Fig. 1 Spatial distribution of monthly mean (June to September) sea level pressure (hPa, *shaded*) and midtropospheric temperature (K, *contours*) for **a–d** model, **e–h** ERAI and **i–l** bias (model minus ERAI)

Table 2 Pattern correlation of different fields between model and observations

Pattern correlation	Rainfall (model vs. GPCP)	Midtropospheric temperature (model vs. ERAI)	Low (upper) level winds (model vs. ERAI)	SLP (model vs. ERAI)
June	0.60	0.8	0.66 (0.87)	0.77
July	0.48	0.56	0.64 (0.73)	0.71
August	0.28	0.65	0.49 (0.57)	0.55
September	0.32	0.86	0.43 (0.62)	0.58
JJAS	0.42	0.76	0.55 (0.70)	0.63

analysis, model simulated fields are compared with NCEP FNL. Figure 4 illustrates the monthly mean low level (850 hPa) wind fields from model (a–d) and NCEP FNL (e–h). The features of ridge line on the western parts of southern peninsular India are well simulated. The model also captures the presence of systematic trough line off west coast of India (causes heavy precipitation), which is not apparent in the parent analysis. Figure 5 illustrates the monthly mean low level (850 hPa) wind fields from model (a–d) and NCEP FNL (e–h). The monthly evolution of mean monsoon flow in model strengthens during peak monsoon months over the western AS and is in agreement with that of NCEP FNL fields but low level jet is slightly broader. The model simulated wind field shows a well-defined cyclonic circulation over the MCR along the Indo-gangetic plains (circulation with westerlies on the southern flanks and easterly winds on the northern flanks of the MT) which is not seen in the parent analysis. The cyclonic circulation of monsoonal winds over Bay of Bengal (BoB) can be noticed unlike in NCEP FNL data. Model could simulate upper tropospheric circulation features which include the Tibetan anticyclone and the TEJ in agreement with NCEP FNL data (figure is not shown). It is interesting to see that anticyclonic circulation and its position over the northeastern states of India with well-defined system is captured by the model unlike in NCEP FNL data. Model could simulate the mean subtropical westerly jet as seen in the corresponding parent analysis. Some of these results are very similar with ERAI. Overall, it is clear that model could produce fine scale features.

Spatial distribution of monthly mean precipitation from model (a–d), GPCP (e–h) and bias (i–l) are displayed in Fig. 6. The model is able to capture the major convective centers over the eastern AS, BoB, MCR and, south China and Philippine Sea as in observations. It is important to note that the model captures the finer details of orographic precipitation along the Himalayan foothills, which are not seen in observations. Unrealistic Inter Tropical Convergence Zone (ITCZ) pattern is evident in the region south of equator from June to September. The strong moisture advection over Indian land mass from head BoB and western Pacific is leading to excess rainfall over MCR. Ratnam

et al. (2009) reported that the prescribed SSTs can also lead to wet bias in the RCMs. The Mean Absolute Error (MAE) and Root Mean Square Error (RMSE) are computed using daily rainfall data at each grid point with respect to observations (Figure not shown). It clearly indicates that the model has wet bias (RMSE (MAE) of 10 (8) mm day^{-1}) over the west coast of India and BoB and it is significantly less over the MCR. Further, analysis reveals that the monthly evolution of monsoon characteristics is reproduced by the model reasonably well. The PC of all these features is provided in Table 2. However, some notable discrepancies are found in the simulated mean features of ISM in the model. Over all bias/error analysis reveals relatively minimum errors in precipitation over the MCR and large errors over oceanic region. In order to examine the model fidelity in simulating the time evolution of rainfall over MCR, the daily rainfall climatology is computed for the period of 2001–2011 (Fig. 7a). The model simulated seasonal cycle is compared with GPCP and TRMM observed rainfall. The model precipitation is overestimated during the peak monsoon phase whereas onset and withdrawal phases are found to be consistent with the observations. The model statistics over land are calculated based on the IMD gridded rainfall and TRMM satellite data. Model error statistics such as mean, standard deviation (SD), correlation coefficient (CC), bias and RMSE are provided in Tables 3 and 4. Analysis indicates that model has good correlation (0.7) with IMD rainfall but higher variability. Further, assessment of the model monsoon rainfall is carried out over the five major sub-divisions of Indian subcontinent (Table 5) (Mooley and Parthasarathy 1984; Srinivas et al. 2012). Analysis shows minimum bias (0.4 mm day^{-1}) and RMSE (2.3 mm day^{-1}) over MCR and maximum bias (10.7 mm day^{-1}) and RMSE (12.2 mm day^{-1}) over south eastern region followed by Western Ghats region (moderate bias of 4.8 mm day^{-1} and RMSE of 7 mm day^{-1}). Model has dry bias over north eastern region (bias of −0.4 mm day^{-1}) and north western region (bias of −0.3 mm day^{-1}). The rainfall skill of the model for different categories is exhibited by TS analysis (Table 6). Model produced low and moderate rainfall categories are relatively better than the high rainfall category. Figure 7b–d is the time latitude section
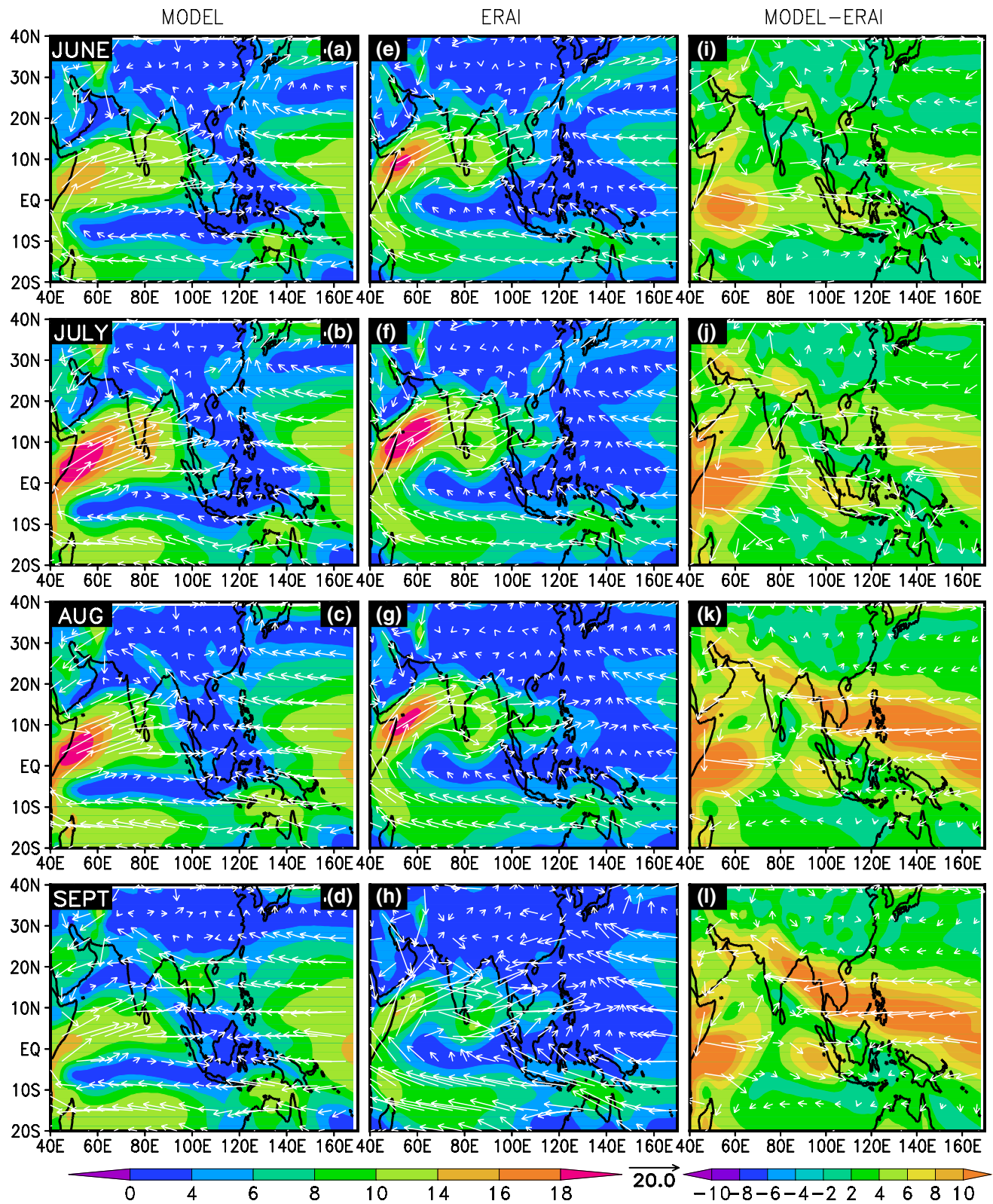
Fig. 2 Spatial distribution of monthly mean (June to September) low level wind (850 hPa) speed (ms^{-1}, *shaded*) and direction (*vectors*) for **a–d** model, **e–h** ERAI and **i–l** bias (model minus ERAI)
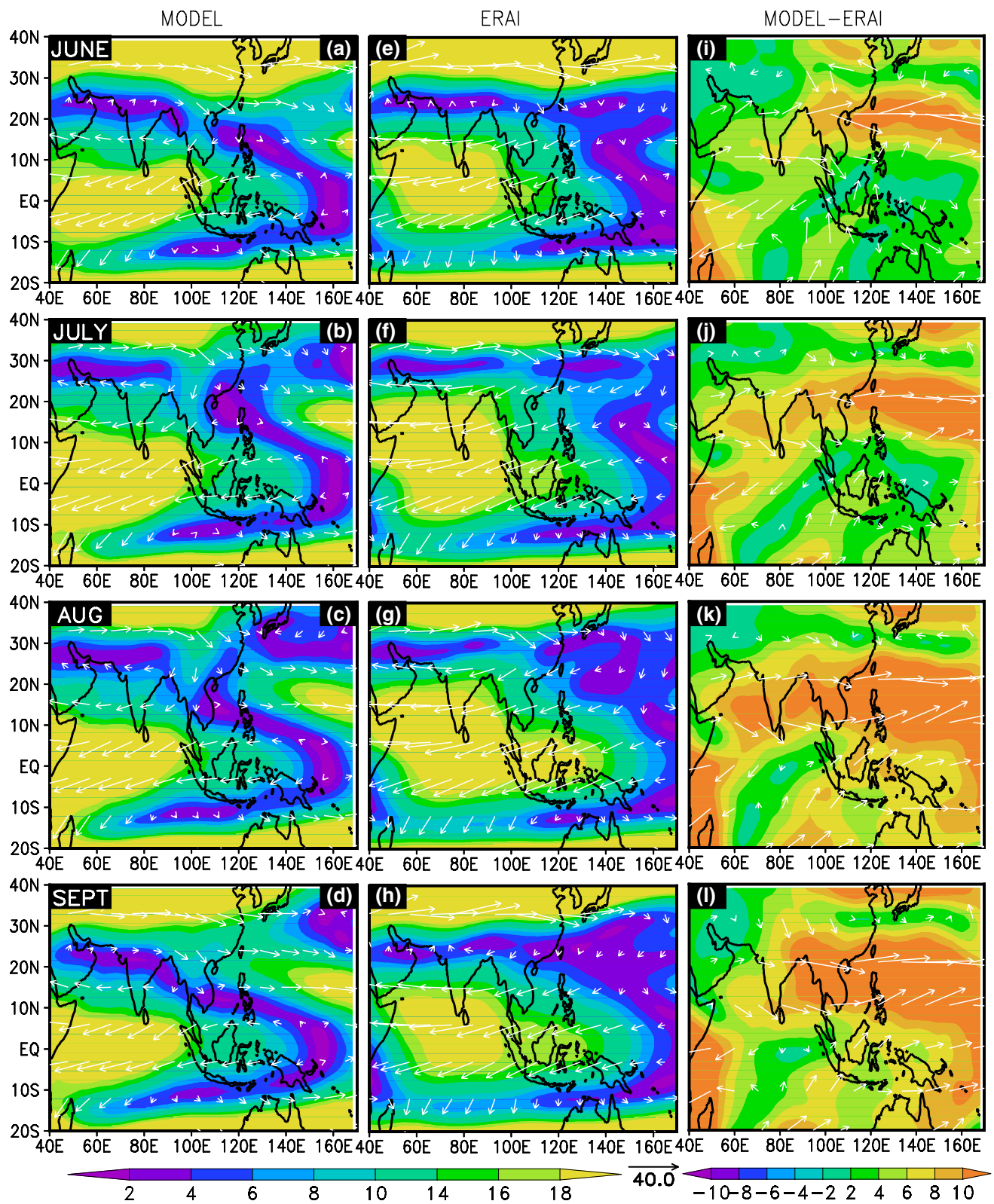
Fig. 3 Spatial distribution of monthly mean (June to September) upper level wind (200 hPa) speed (ms^{-1}, *shaded*), direction (*vectors*) for **a–d** model, **e–h** ERAI and **i–l** bias (model minus ERAI)
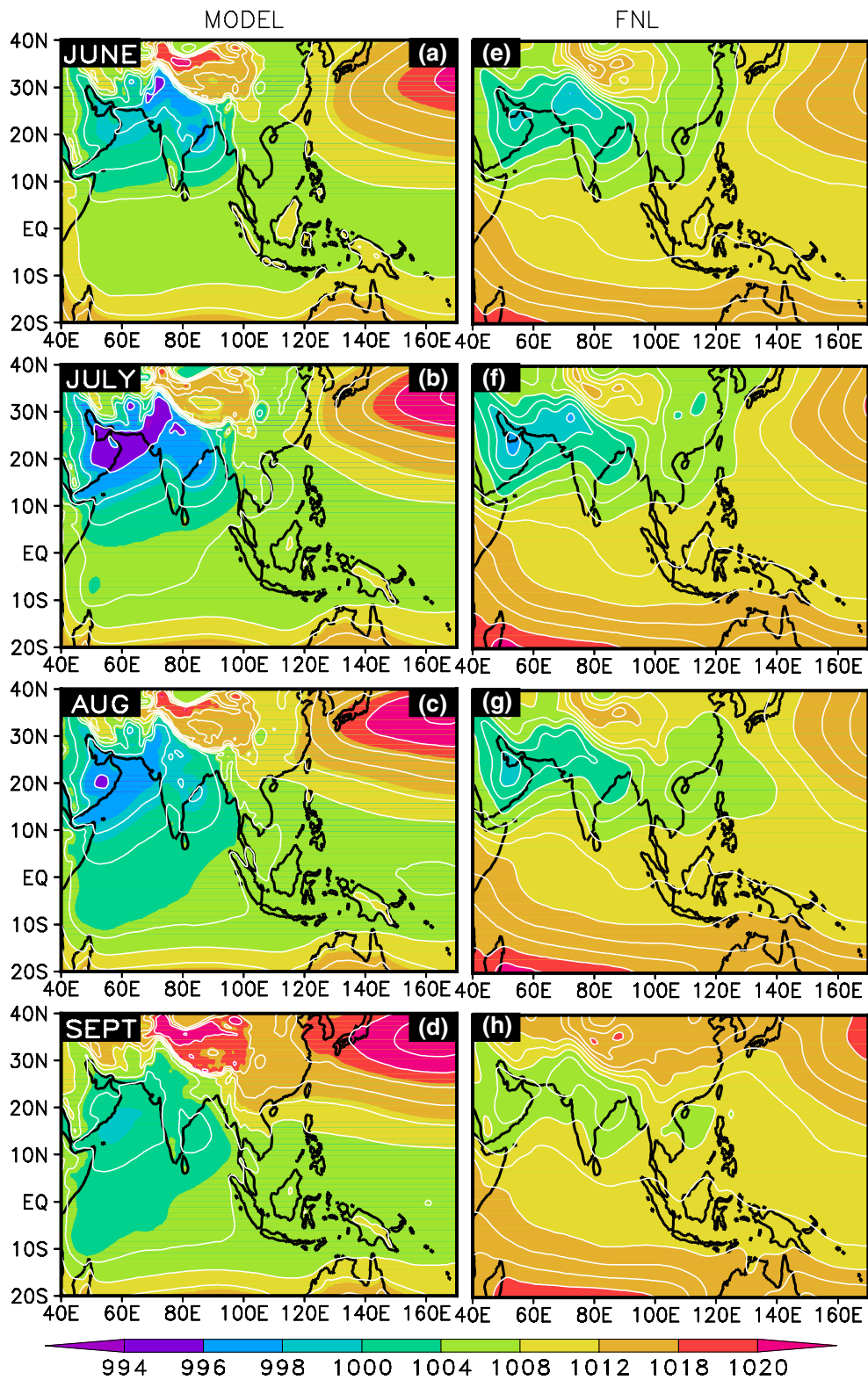
Fig. 4 Spatial distribution of monthly mean (June to September) sea level pressure (hPa, *shaded*) for **a–d** model, **e–h** NCEP FNL
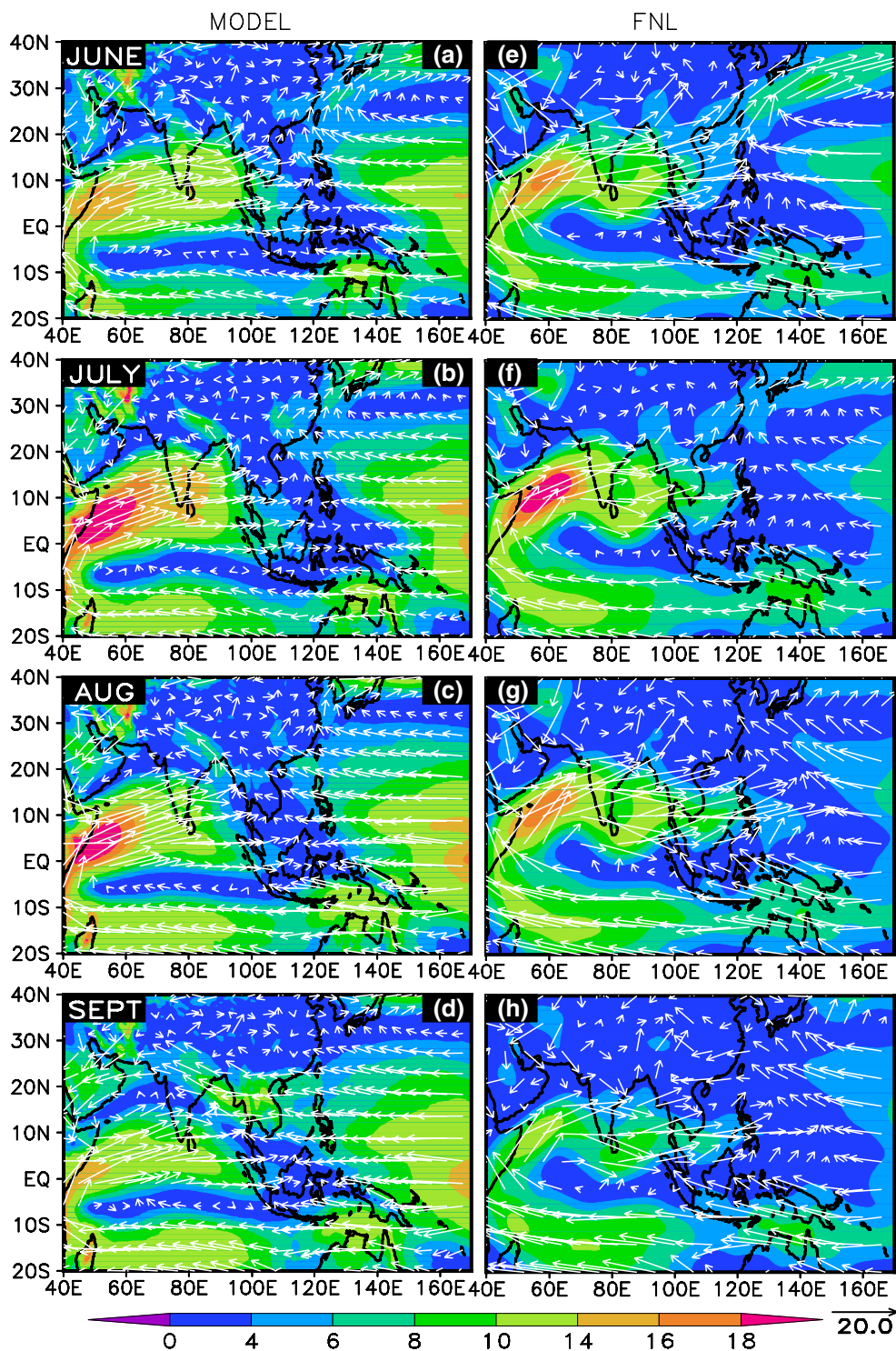
Fig. 5 Spatial distribution of monthly mean (June to September) low level wind (850 hPa) speed (ms^{-1}, *shaded*) and direction (*vectors*) for **a–d** model, **e–h** NCEP FNL

of daily precipitation (mm day^{-1}) averaged over the land region (70–90°E) for model, GPCP and TRMM during the monsoon season. The daily rainfall is normalized with maximum precipitation (contours above 0.4) to see the

northward extend of the maximum rain band in the model and observations. The seasonal evolution of northward propagation of maximum rain band is found to be reasonably good. The model simulated rainfall appears higher
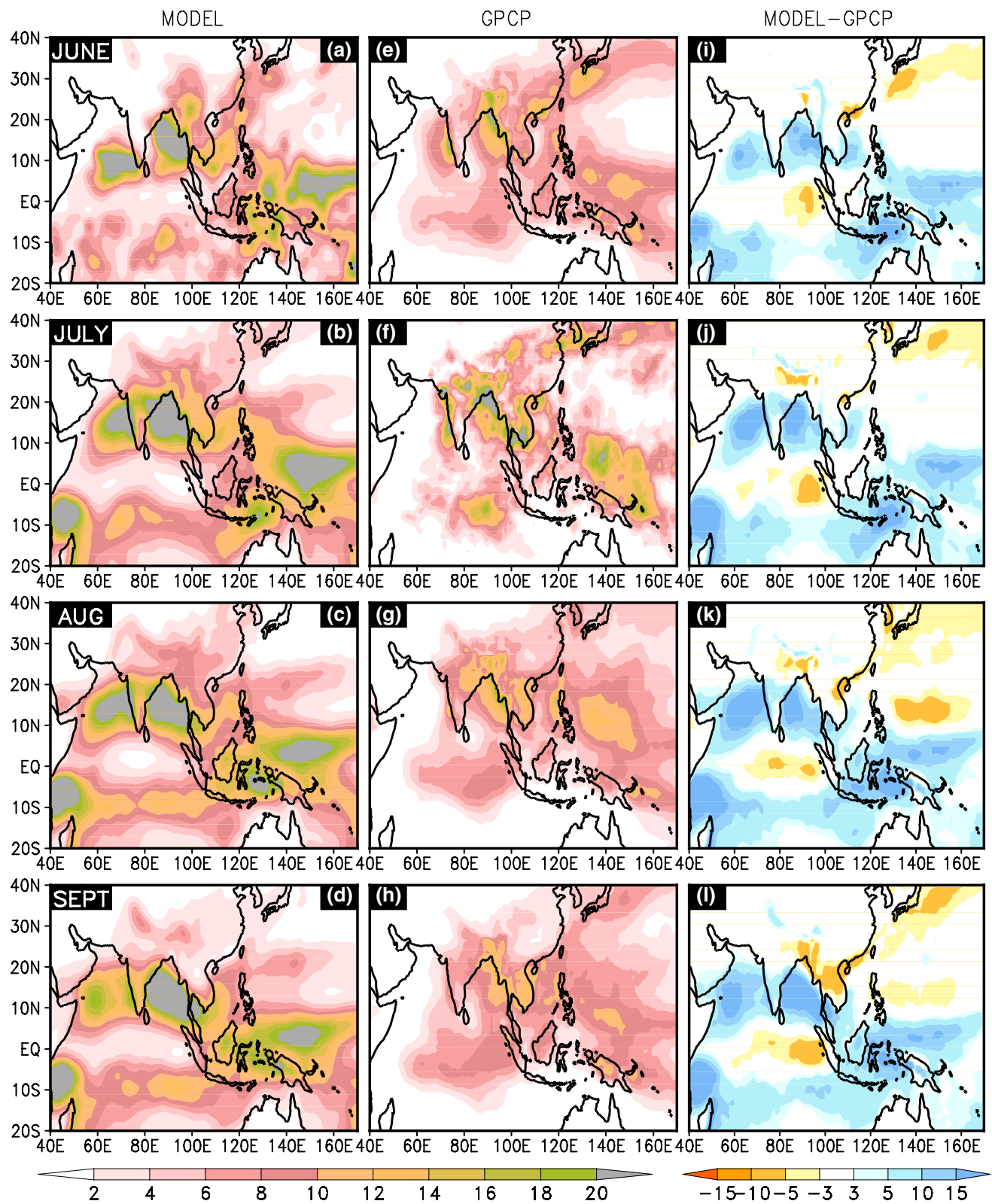
Fig. 6 Spatial distribution of monthly mean (June to September) rainfall (mm day^{-1}) for **a–d** model, **e–h** GPCP and **i–l** bias (model minus GPCP)
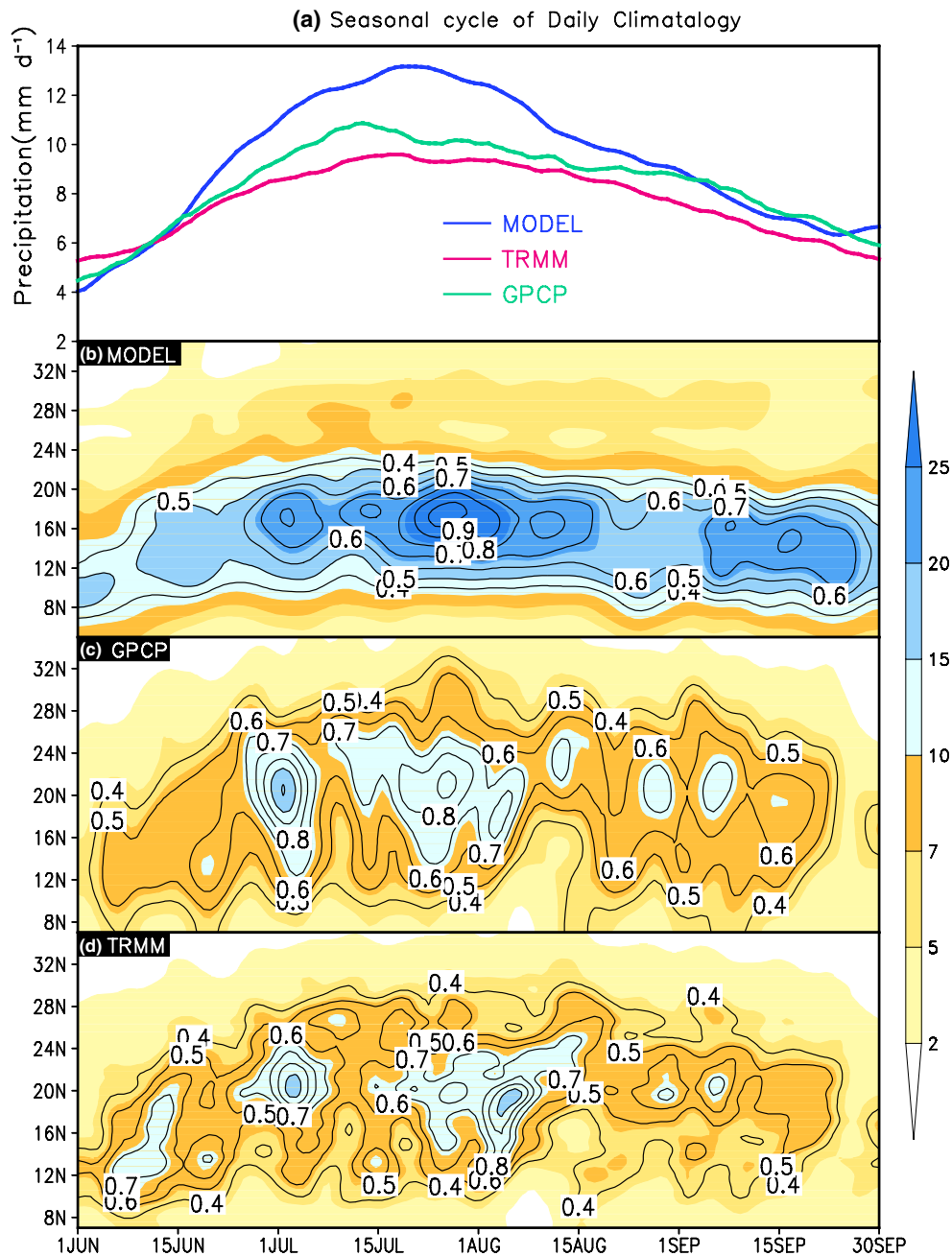
Fig. 7 **a** Seasonal evolution of area averaged rainfall (mm day^{-1}) over the MCR. The time-latitude section of rainfall (mm day^{-1}; *shaded*) and normalized rainfall (*contours*) averaged over the region (70–90°E) for **b** model, **c** GPCP and **d** TRMM. Here daily climatology of rainfall is based on period 2001–2011

Table 3 Mean monsoon rainfall (mm day^{-1}) and its standard deviation (mm day^{-1}) averaged over the MCR for individual months and season from model, IMD and TRMM

Mean (SD)	June	July	August	Sept	JJAS
Model	5.5 (2.3)	12.1 (2.1)	9.5 (1.6)	6.3 (1.9)	8.4 (3.3)
IMD	4.9 (2.7)	9.3 (1.6)	9.1 (1.5)	7.1 (2.0)	7.7 (2.6)
TRMM	6.5 (2.1)	10.8 (2.6)	9.4 (1.9)	6.9 (2.0)	8.5 (2.8)

than the IMD and TRMM observed rainfall, and the model maximum rain band extends only up to 23°N whereas it reached up to 28°N in observations. The meridional asymmetric bias of SLP, leading to weaker vertical wind shear, is limiting the northward migration of maximum rain band. To understand the possible causes for precipitation biases in the model, we analyzed the vertical structure of dynamic and thermodynamic parameters in the following section.

Table 4 Correlation coefficient, Bias (mm day^{-1}, given in bracket) and Root Mean Square Error (mm day^{-1}) of model simulated rainfall over the MCR with IMD and TRMM for individual months and whole season

CC (Bias)	June	July	August	Sept	JJAS
Model vs. IMD	0.9 (0.4)	0.5 (2.8)	0.7 (0.3)	0.1 (−0.7)	0.7 (0.7)
Model vs. TRMM	0.8 (−1.05)	0.6 (1.3)	0.6 (0.09)	0.7 (−0.6)	0.6 (−0.05)
RMSE	June	July	August	Sept	JJAS
Model vs. IMD	1.1	3.4	1.1	2.6	2.3
Model vs. TRMM	1.5	3.4	1.8	2.8	2.5

Table 5 Statistical skill scores for model seasonal mean rainfall against to IMD observed rainfall over different sub-regions of Indian subcontinent

Zone	Mean (mm day^{-1}) model (IMD)	STD (mm day^{-1}) model (IMD)	Bias (mm day^{-1})	RMSE (mm day^{-1})	CC
MCR	8.4 (7.7)	3.3 (2.6)	0.7	2.3	0.7
WGR	18 (13.5)	4.3 (4.8)	4.8	7.04	0.35
SER	15.9 (5.2)	6.3 (2.2)	10.7	12.2	0.3
NER	8.8 (9.2)	4.2 (2.7)	−0.4	4.7	0.15
NWR	6.5 (6.9)	4.8 (4.4)	−0.3	5.1	0.38

Table 6 Threat scores for model rainfall with respect to IMD (TRMM) observations over MCR

Rainfall (mm day^{-1})	IMD (TRMM)	Model	Hits	Threat score
Low (<5)	19 (15)	22	6 (4)	0.17 (0.12)
Moderate (5–10)	83 (73)	61	20 (13)	0.16 (0.10)
High (≥10)	20 (34)	39	7 (5)	0.13 (0.07)

4 Vertical structures of dynamic and thermodynamic parameters

This section describes the vertical structures of the dynamic (zonal, meridional and vertical winds, vorticity and divergence) and thermodynamic (Temperature, WVMR and Equivalent Potential Temperature) parameters associated with ISM over MCR. Assessment of these parameters associated with ISM in the model is important to reveal the model deficiencies for realistic simulations.

4.1 Temperature, moisture and equivalent potential temperature

Vertical structure of temperature associated with ISM has coherent response to precipitation strength at middle and lower troposphere. Mean vertical profiles of temperature and time-height cross section of temperature anomalies with rainfall anomalies during ISM over MCR from model and AIRS are shown in Fig. 8a. The mean vertical profile of temperature from model and observations (right panel in Fig. 8a) displays good resemblance with each other in terms of vertical structure. The temperature and rainfall anomalies are obtained by removing their seasonal mean. The boundary layer is warmer (1.5–2 K) than the observed

during the first 3 weeks of June whereas middle to upper troposphere is cooler (1–1.5 K). While during July and August strong warming from middle to upper troposphere and the corresponding cooling in the boundary layer is evident in observations and model, which is consistent with the precipitation variability. AIRS observations show relatively higher boundary layer cooling during the convective phase and its vertical extent of warming associated with precipitation is shallower (600–300 hPa) and with the progression of the season it extends up to 400 hPa. Whereas in the model vertical extent does not show any change with the progression of the season and the vertical extent is quite deep (up to 200 hPa) under the high precipitation conditions. The model is produced stronger midtropospheric temperature anomalies than AIRS, which are due to overestimation of latent heat associated with the inherent wet bias. On the other hand the boundary layer warm bias during ISM over the MCR is due to the underestimation of evaporative cooling in the model. Thus, baroclinic response of temperature is weaker during July and August in the model compared to that of AIRS.

Vertical structure of WVMR associated with monsoon is important for the lower to midtropospheric instability, midtropospheric heating and circulation. Thus, the assessment of moisture associated with ISM over MCR in the model is vital. Mean vertical profile and time-height cross section of WVMR anomalies along with the rainfall anomalies during ISM over MCR from model and AIRS are shown Fig. 8b. Model mean profiles of WVMR in free troposphere are consistent with that of AIRS but slightly away in lower troposphere. This further deduces that the model vertical profile of WVMR decreases gradually as in AIRS observations in the lower troposphere. The dry bias of WVMR in the boundary layer may be due to the underestimation of
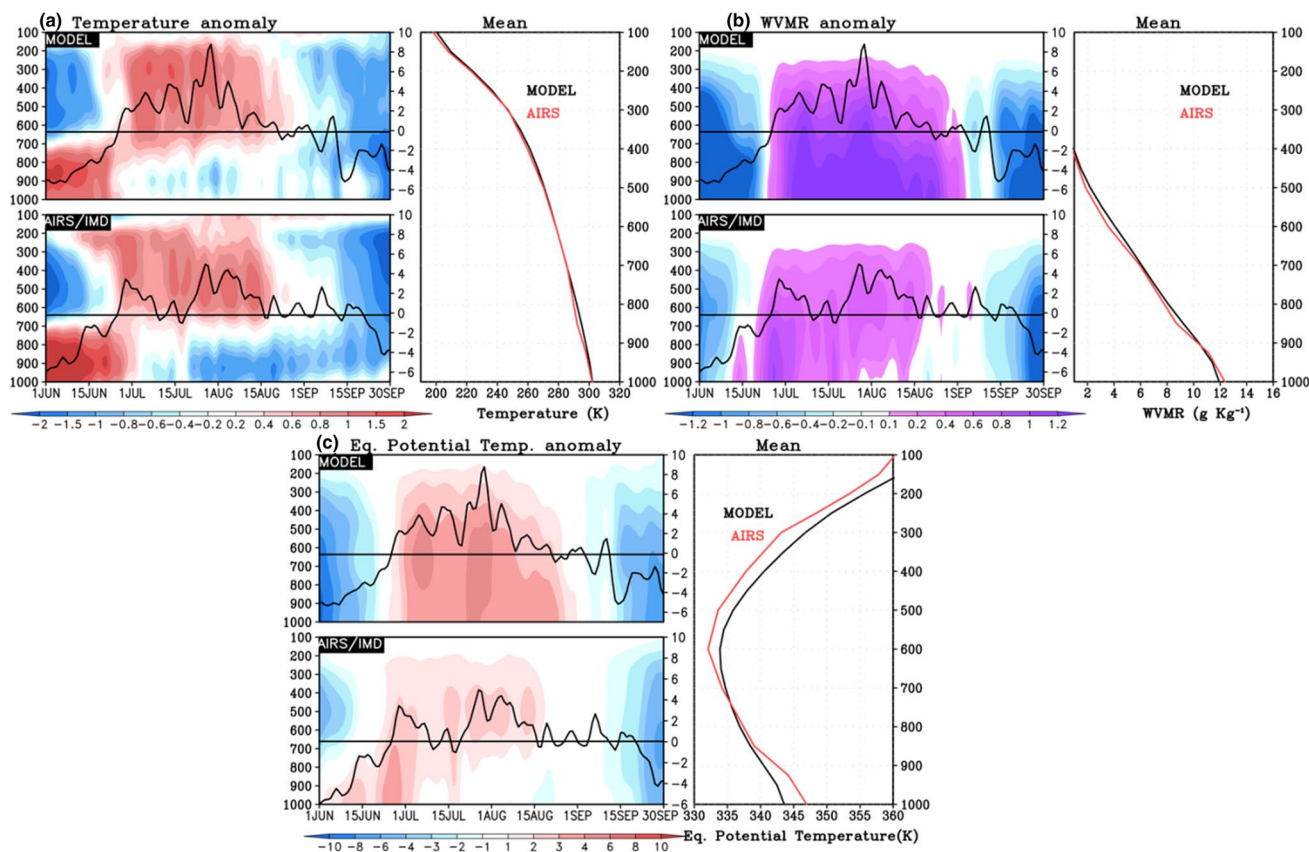
Fig. 8 Time-height cross section of anomaly (*shaded*, *left panels*) and mean *vertical* profiles (*right panels*) over MCR from model (*black*) and AIRS (*red*) for **a** Temperature (K), **b** WVMR (g Kg^{-1}) and **c** Equivalent potential temperature (K). Rainfall anomaly (mm day^{-1}, *solid line* and scales at *right*) overlaid on time-height cross section (*left panels*) from June to September

surface evaporation, which is consistent with surface warm bias. The time-height cross section of moisture anomalies corresponding to the rainfall anomalies associated with ISM over MCR from model and AIRS reveals negative moisture anomalies during the onset and withdrawal phases of monsoon, and positive anomalies during the peak monsoon period. These features are well simulated by the model. However, the model WVMR anomalies are negative till the third week of June and vertical extent is up to 200 hPa, while it has strong positive anomalies during July and August. These positive anomalies of WVMR are consistent with that of AIRS observed anomalies with slightly higher magnitude. The vertical extent of positive WVMR anomalies is found to be deeper in the model than observations. Overall the model has wet bias during the peak monsoon, due to strong easterly bias which brings excess moisture from western Pacific and BoB to MCR.

Equivalent potential temperature (EPT) is a measure of instability. Normally EPT increases (decreases) with the height during the stable (unstable) conditions. The mean vertical profile and time-height cross section of EPT anomalies with rainfall anomalies during ISM over MCR from

model and AIRS are shown Fig. 8c. The model has captured mean vertical structure of EPT as well as systematic evolution of instability during the season. Mean vertical profile of EPT shows that the model and AIRS have similar nature throughout the troposphere with significant differences in the lower and upper troposphere (right panel in Fig. 8c). AIRS observations show that the rate of decrease of EPT with the height in the low to midtroposphere is sharper over MCR while such sharpness is absent in the model (vertical gradient between 1,000 and 600 hPa is weaker by 1.5 times than observations). This vertical gradient of EPT indicates that model is more stable than AIRS at low levels. The profile of EPT supports that the model simulated a more unstable atmosphere in the midtroposphere than AIRS, leading to the positive bias of rainfall. The model has a weak EPT in the lower troposphere (up to 700 hPa) and strong EPT in the middle to upper troposphere (150 hPa) compared to AIRS. This weak EPT in the lower troposphere is mainly due to underestimation of WVMR due to local evaporation (Fig. 8b). Whereas, the strong EPT at higher levels is primarily caused by temperature and midlevel moistening due to advection. The seasonal evolution of EPT anomaly

is positive during the peak phase of monsoon and negative during the onset and withdrawal phases (left panel in Fig. 8c). This indicates that model has stronger instability than observations during the convective phase. The strong instability in the lower to midtroposphere potentially pumps up moisture to the deeper extent resulting positive precipitation and warmer midtropospheric temperature anomaly in the model than observations.

4.2 Zonal and meridional wind

Conventionally, the zonal wind shear is one of the fundamental measures of the strength of ISM and is closely linked geostrophically to the temperature by the thermal wind relation (Holton 2004). Vertical structure of horizontal winds mainly follows baroclinic nature during ISM. Figure 9a shows the vertical distribution of mean zonal wind and time-height cross section of zonal wind anomalies superimposed by rainfall anomalies over the MCR from model and ERAI during ISM. It is found that model has weak westerly winds (<1 m s^{-1}) in the lower troposphere (below 900 hPa) and easterlies above it, while strong westerlies (4 m s^{-1}) with vertical extent up to 600 hPa and easterlies above is reported in ERAI. Thus model underestimates mean monsoon zonal flow in the entire troposphere and the vertical shear of zonal wind (Fig. 9a). The strength and vertical extent of zonal wind shear are important for the northward propagation of the intraseasonal oscillations (e.g. Jiang et al. 2004). Temporal variability of zonal wind anomalies is shown in Fig. 9a (left panel). Model could produce strong westerlies (easterlies) in the lower (upper) troposphere associated with strong precipitation till the end of July while ERAI shows this till the end of August. Thus vertical shear of zonal wind anomaly is improper in the model during August. During the withdrawal phase of monsoon, lower tropospheric easterly anomalies and upper tropospheric westerly anomalies appeared in the model and ERAI.

Mean vertical profiles of meridional wind and time height cross section of meridional wind anomalies associated with the rainfall over MCR from model and ERAI are shown in Fig. 9b. The time mean vertical structure of meridional wind in the model shows slightly strong southerlies in the lower and upper troposphere and weak northerlies in the midtroposphere than ERAI (right panel in Fig. 9b). So, the model underestimates meridional wind shear compared to ERAI. Figure 9b (left panel) shows the seasonal evolution of meridional wind and precipitation anomalies from model and ERAI. Model shows northerly wind anomalies till the end of July with vertical extent up to 300 hPa, while rest of the season it is southerly. But in the case of ERAI, the boundary layer has southerly till mid-August with the vertical extent from 800 to 500 hPa. Thus model underestimates zonal and meridional wind shear over the MCR.

4.3 Vertical wind velocity, vorticity and divergence

Figure 9c illustrates the mean profile of vertical wind and time height cross section of vertical wind anomalies with precipitation anomalies over MCR from the model and ERAI. Mean profiles of vertical velocities during JJAS is in agreement with the ERAI over MCR (Fig. 9c). Analysis deduced that the model and ERAI display negative vertical velocity in the boundary layer (up to 900 hPa) and positive vertical velocity from 800 to 200 hPa. In the case of model, vertical velocities are overestimated above 800 hPa (Fig. 9c). In the midtroposphere negative vertical velocity anomalies are reported during the onset and withdrawal phases of the monsoon whereas positive vertical velocity anomalies are noted during the peak monsoon phase in both model and ERAI. The strong upward motion is resulting from the strong moist unstable atmosphere whereas negative vertical velocities may be due to dry low level conditions. Strong vertical velocity (extending up to 100 hPa) associated with strong precipitation is reported by the model with overestimation in the middle to upper troposphere. This may be due to high Convective Available Potential Energy (CAPE) in the model associated with the strong water vapor loading, supporting instability in the middle troposphere to upper troposphere.

Mean profiles of vorticity and time height cross section of its anomalies associated with rainfall anomalies over MCR are shown in Fig. 9d. During monsoon strong low level cyclonic vorticity up to 500 hPa and anticyclonic vorticity aloft is evident in the model as in the observations. Rise of cyclonic vorticity anomalies is evident during the peak monsoon phase, whereas negative vorticity anomalies are seen during the onset and withdrawal stages of the monsoon and is similar to that of ERAI. Latent heating from organized mesoscale convective systems can effectively promote the upward development of continental-scale cyclonic circulation well above the midtropospheric level during ISM (Choudhury and Krishnan 2011). The vertical extent and strength of vorticity anomalies are slightly overestimated in the model during the peak phase of monsoon. Mean profile of divergence and time height cross section of its anomaly associated with rainfall anomalies over MCR are shown Fig. 9e. Time mean divergence profiles in model displays low level convergence and mid to upper tropospheric divergence as in ERAI with slight overestimation in the low level convergence (Fig. 9e). Time height cross section of divergence anomalies over MCR corresponding to rainfall reveals strong upper level divergence and low level convergence during the peak monsoon months in the model and ERAI (Fig. 9e). Low level divergence and upper level convergence are noticed during the onset and withdrawal phases of monsoon in the model and ERAI. Hence the model could simulate the time evolution
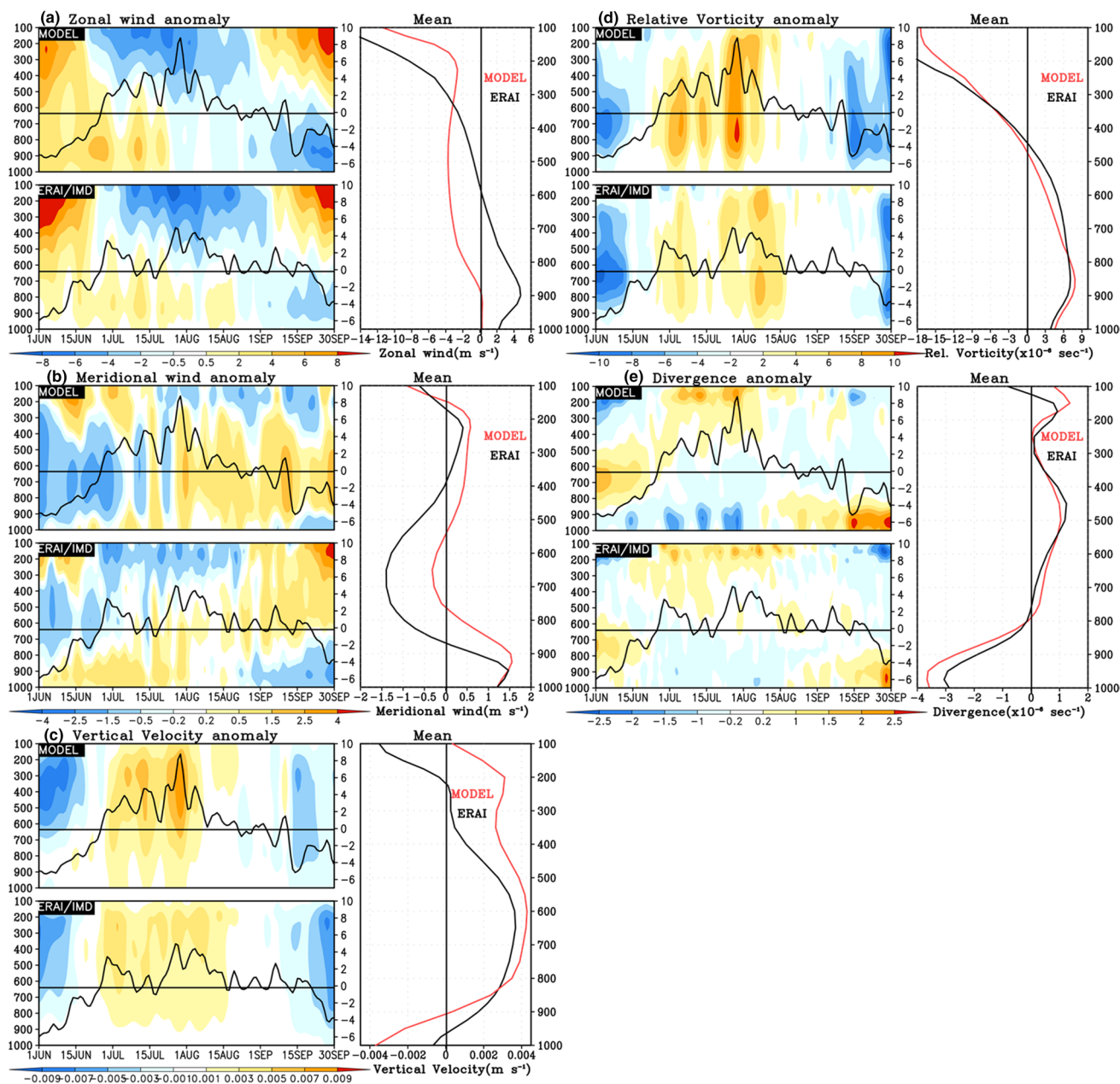
Fig. 9 Time-height cross section of anomaly (*shaded*, *left panels*) and mean *vertical* profiles (*right panels*) over MCR from model (*red*) and ERAI (*black*) for **a** zonal wind (ms^{-1}), **b** meridional wind (ms^{-1}), **c** *vertical* wind (ms^{-1}), **d** relative vorticity ($\times 10^6$ s^{-1}), **e** divergence ($\times 10^6$ s^{-1}). Rainfall anomaly (mm day^{-1}, *solid line* and scales at *right*) overlaid on time-height cross section (*left panels*) from June to September

of divergence structure realistically. But the magnitude is slightly overestimated in the model. Thus the vertical structure of relative vorticity (divergence) associated with ISM is represented reasonably well with overestimation (underestimation) at the lower troposphere in the model. Overall, strong lower level convergence and upper level divergence resulting in enhanced updrafts that supports to moist biases in the precipitation.

5 Assessment of intraseasonal oscillations (ISOs)

Goswami (2005) found that mean ISM has vigorous ISOs, that manifest in the sub-seasonal active and break spells of monsoons. It is well established that during the active and break conditions of ISM, the large scale flow shows different behavior in terms of formation of weather systems, instability and most importantly the rainfall variability (e.g.

Goswami et al. 2003; Taraphdar et al. 2010). The simulation of ISO's associated with ISM is equally important for the credibility of the model (e.g., Krishnamurthy and Shukla 2000). Most of the climate models exhibit difficulty in simulating the ISOs (e.g. Waliser et al. 2003; Goswami et al. 2011). Very few studies attempt to simulate ISO features using the RCM (e.g. Bhaskaran et al. 1998), but none of them explore vertical structure of simulated ISOs. This section describes mean spatial distribution of SLP, circulation and precipitation as well as vertical structure of temperature, WVMR and vorticity during the active and break conditions from the model and observations respectively.

5.1 Spatial structure of precipitation, SLP and winds during ISOs

In order to examine the fidelity of model in simulating the ISOs, we have identified the total number of 13 (17) active and 10 (13) break cases based on the precipitation index (Rajeevan et al. 2010) from IMD (model) rainfall data during the study period. This indicates that model has relatively more active and break events than observations. The composite of rainfall, SLP and low level winds during the active and break spells are shown in Fig. 10 for the model (upper panel) and ERAI (bottom panel) respectively. Major features of the active phase are formation of low SLP anomalies over northwest and central India, strong southwesterly wind anomalies at the low level, southward shifting of monsoon trough from its normal position and excess rainfall over the MCR (Fig. 10b). Model could simulate these features reasonably well compared to observations during the active phase (Fig. 10a). Negative precipitation anomalies over the equatorial region and southern peninsula of India are seen in the model, however model missed negative precipitation near the foot hills of Himalaya associated with active monsoon. Strong precipitation over Burma and western Pacific are well simulated in the model. Thus model captures the active phase characteristics over the MCR and the associated features over the Indian Ocean and adjacent land mass.

The low level anticyclonic wind anomalies over India and weak trough over the foothills of Himalayas and low level cyclonic anomalies over northwest Pacific region are seen during the break phase in ERAI (Fig. 10d). During the break phase the model produces the spatial variability of precipitation, SLP and low level winds reasonably well. The model produced strong negative rainfall anomalies over the MCR and associated high SLP (Fig. 10c).
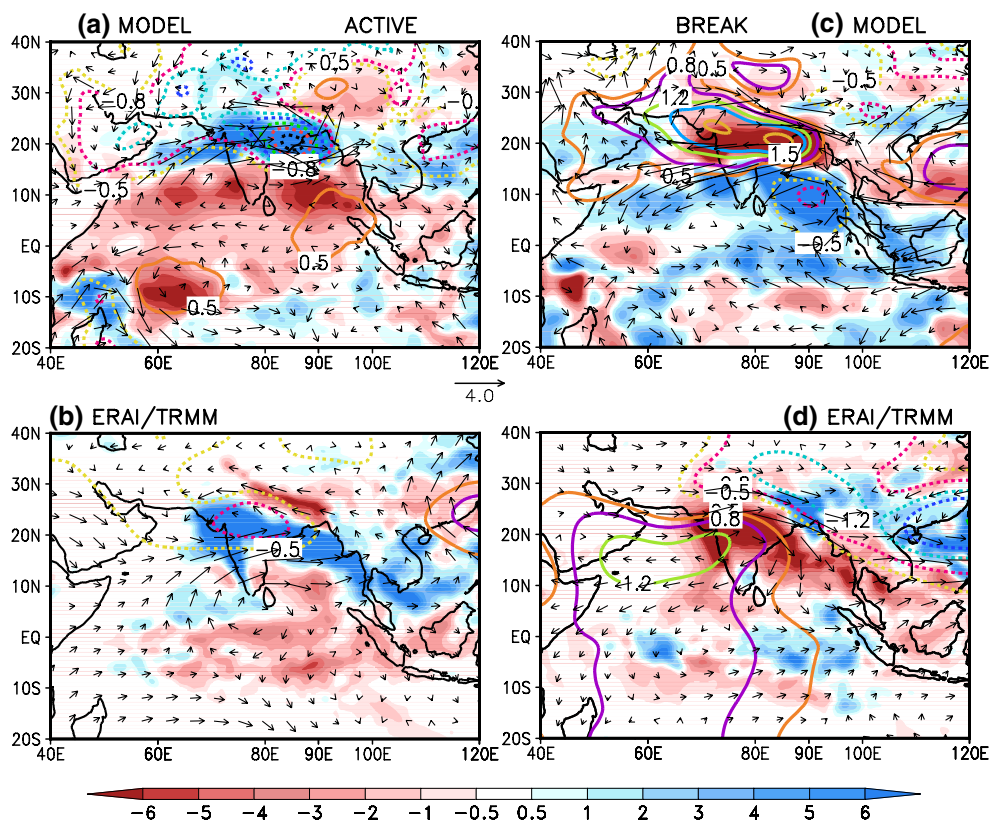

Fig. 10 Composite of precipitation (mm day^{-1}, *shaded*), SLP (hPa, *contours*) and low level winds (ms^{-1}, *vectors*, at 850 hPa) for active phases **a** model and **b** ERAI/TRMM, for break phases **c** model and **d** ERAI/TRMM

The low level anticyclonic wind anomalies over India and anomalous easterlies in the AS support major reduction in moisture transport to MCR, indicating weak monsoon circulation. These features are well represented in the model but overestimates SLP and low level wind anomalies. The model simulated strong precipitation anomaly associated with the break extended up to 15°N, whereas it is confined to the eastern equatorial Indian Ocean in the observations (Fig. 10d). Model simulated unrealistic cyclonic circulation over the BoB under the break condition, is responsible for positive rainfall anomaly up to 15° N. Further model missed positive precipitation anomaly over the foot hills of Himalaya during the break phase. Hence, the spatial structure of active and break spells of ISM are simulated by the model reasonably good. Further analysis suggests that the large scale features associated with breaks are better simulated by the model than active phase.

5.2 Vertical structure of temperature, WVMR and vorticity during ISO

In this section, we evaluate the lead-lag evolution of moist thermodynamic structures associated with the rainfall during active and break phases. The temperature, WVMR and relative vorticity anomalies are computed for 15 days before and 15 days after the respective day of the peak intraseasonal rainfall for each phase. Figure 11 portrays the composite of vertical structure of temperature anomaly over the MCR from model (a–d), AIRS (b–e) and ERAI (c–f) for the active and break phases of monsoon, where precipitation anomaly (time series) is overlaid. Model shows negative anomalies in the lower troposphere and positive anomalies above 700 hPa at the peak phase of rainfall (Fig. 11a). Model simulated temperature anomalies show warming (cooling) in the midtroposphere (lower troposphere) about two pentads before and after 1 pentad from the peak phase of intraseasonal rainfall. In the case of AIRS observations (Fig. 11b), during the peak phase (developing phase) of active condition lower troposphere cools (warms) by about 1 K. This cooling in the lower troposphere persists almost up to two pentads from peak rainfall. The vertical extent of midtropospheric warming associated with precipitation is up to 200 hPa in AIRS. Thus vertical structure of temperature in AIRS evolved systematically with the precipitation strength. Similar vertical temperature response during the active phase is evident in ERAI (Fig. 11c). Overall, during active phase the strong warm (weak) anomalies in the lower (mid) troposphere are found at 3 pentad before the precipitation maximum in AIRS (Fig. 11b) and ERAI (Fig. 11c). This condition leads to unstable atmosphere by increasing CAPE (e.g. Fu et al. 2006; Wong et al. 2011). Such preconditioning in the lower troposphere is absent in the model which might be responsible for weak convergence and

thus leads to the underestimation of rainfall over MCR at the peak time. The corresponding baroclinic response of temperature is weaker in the model than AIRS and ERAI. Hence model failed to capture the exact nature of enhanced convection during active phase. Figure 11d shows the vertical structure of temperature anomalies in model during the suppressed convective (break) period. Model shows strong lower tropospheric warming (>1 K), which persists up to two pentads and associated cooling is reported in the midtroposphere (600–200 hPa) with peak at 300 hPa and it persists up to two pentads. In the case of AIRS and ERAI (Fig. 11e, f), vertical temperature response during this phase is in resemblance with each other. Strong upper tropospheric warming and weak lower tropospheric cooling are evident one pentad before the peak time of suppressed convection, on the other hand lower troposphere warming (>0.8 K) and midtroposphere cooling over MCR are evident during the break phase at day 0. This warming at surface is due to sinking motion associated with the break. Vertical extent of cooling is relatively shallow in AIRS and ERAI than model and is persisting for one to two pentads. Thus model vertical temperature structure response to precipitation is different from ERAI and AIRS at the intraseasonal time scales. This strong warming in the boundary layer indicates that there is a lack of feedback from land surface processes and boundary layer physics in the model which needs to be improved. Overall, the model temperature anomalies exhibit almost bimodal vertical structure, that is warm (cold) anomalies in the free troposphere (700–100 hPa) and cold (warm) anomalies in the lower troposphere (below 700 hPa) associated with enhanced (suppressed) convection over MCR though significant differences are evident especially in the boundary layer.

Figure 12 displays composite of vertical structure of WVMR anomalies from model, AIRS and ERAI during the enhanced (active) and suppressed (break) convective phases. Model displays positive anomalies of WVMR throughout the active phase with strong WVMR loading in the lower troposphere on peak day and about 2 pentads ahead (Fig. 12a). During the peak active phase, vertical extent of WVMR is up to 400 hPa. AIRS observations (Fig. 12b) display positive WVMR anomaly during the developing active phase, maximum positive anomaly of WVMR is confined to the lower troposphere 1 pentad ahead of peak phase and vertical extent of WVMR anomaly gradually increased from 3 pentad onwards and highest extent is up to 350 hPa (850–350 hPa). In the case of ERAI (Fig. 12c) WVMR anomaly is positive during the developing phase of active, but maximum strength is 2 pentads ahead and vertical extent is up to 400 hPa. During the decaying phase negative WVMR anomaly is found in the midtroposphere, which is weaker than AIRS. This negative
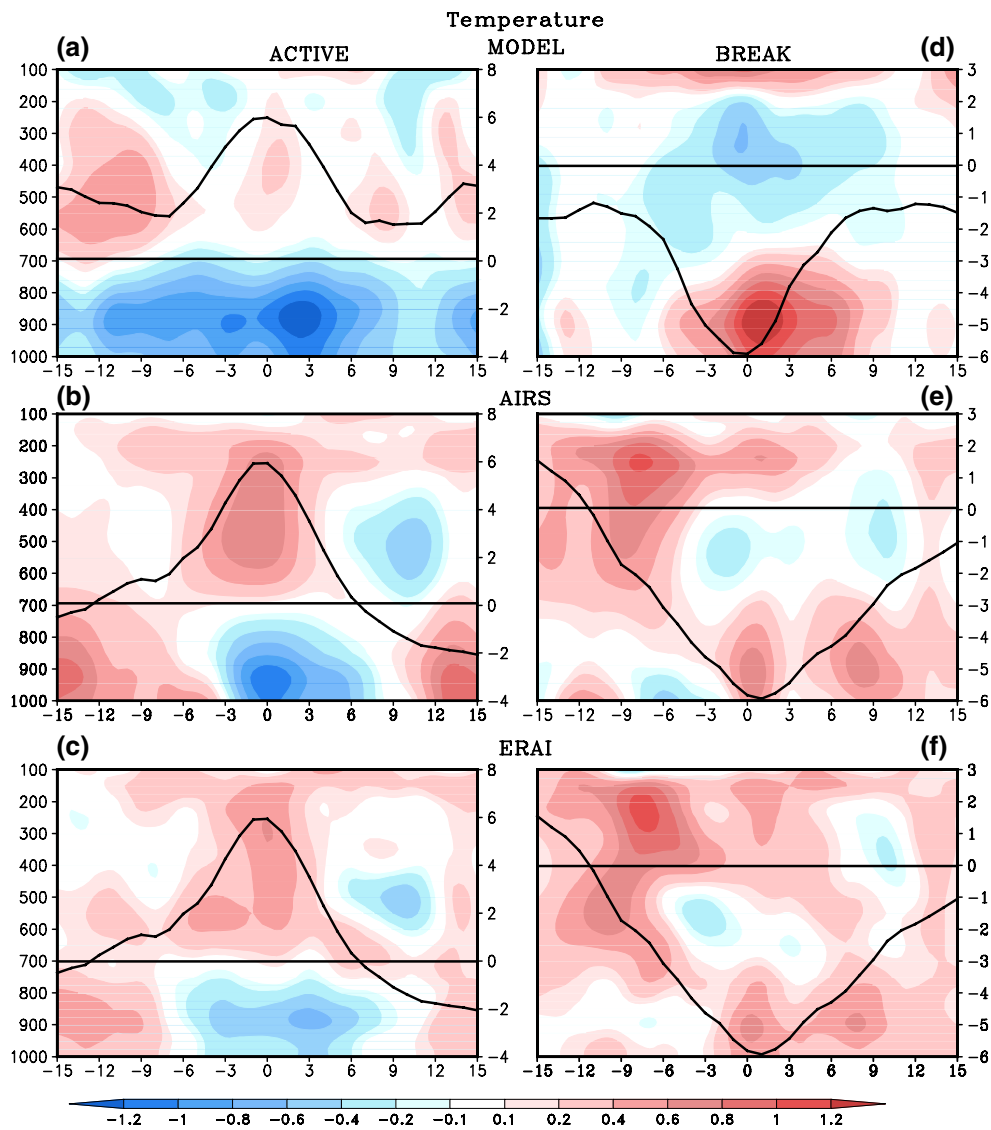
Fig. 11 The lead-lag evolution of composite temperature anomalies (K) averaged over MCR for active (*left panels*) and break (*right panels*) phases from model (**a, d**), AIRS (**b, e**) and ERAI (**c, f**). The overlaid *solid line* represents rainfall anomalies (mm day^{-1}, scales at *right*)

WVMR anomaly remains for the two pentads but does not show vertical expansion with the time as in AIRS. Overall, the water vapor loading begins to develop before peak rainfall, after the passage of peak rainfall there is a sharp drying up of the troposphere, this post convective dryness persists till the next phase begins (in the observation). Such post convective drying is absent in model. This systematic evolution is absent in the model indicating that model has significant biases in the evolution of moist processes during active phase. These biases in the moisture are related to the mean moisture bias in the model. Figure 12d is a vertical response of WVMR during the break phase of monsoon in the model. The model could show the low level drying at peak time of break phase as seen in observations. During break, negative WVMR anomalies are consistent with

the stability of the atmosphere. Negative anomaly in the lower troposphere to 400 hPa is apparent 1 pentad ahead with strong negative WVMR during break maxima. This negative phase persists for the next 2 pentads but its vertical extent gradually comes down to 500 hPa. The vertical response of WVMR from AIRS shows negative WVMR anomalies about 2 pentads ahead of break but its vertical extend is up to 400 hPa (Fig. 12e). Maximum negative anomaly of WVMR occurs 3 days ahead of break and persists for a week. Figure 12f shows the WVMR anomaly from ERAI, strong negative anomaly coincides with the peak of break and has maxima in the 750–600 hPa level and it persists for the next 1 pentad. Thus the systematic evolution of WVMR anomalies in the model is better during break phase compared to active phase. Specifically,
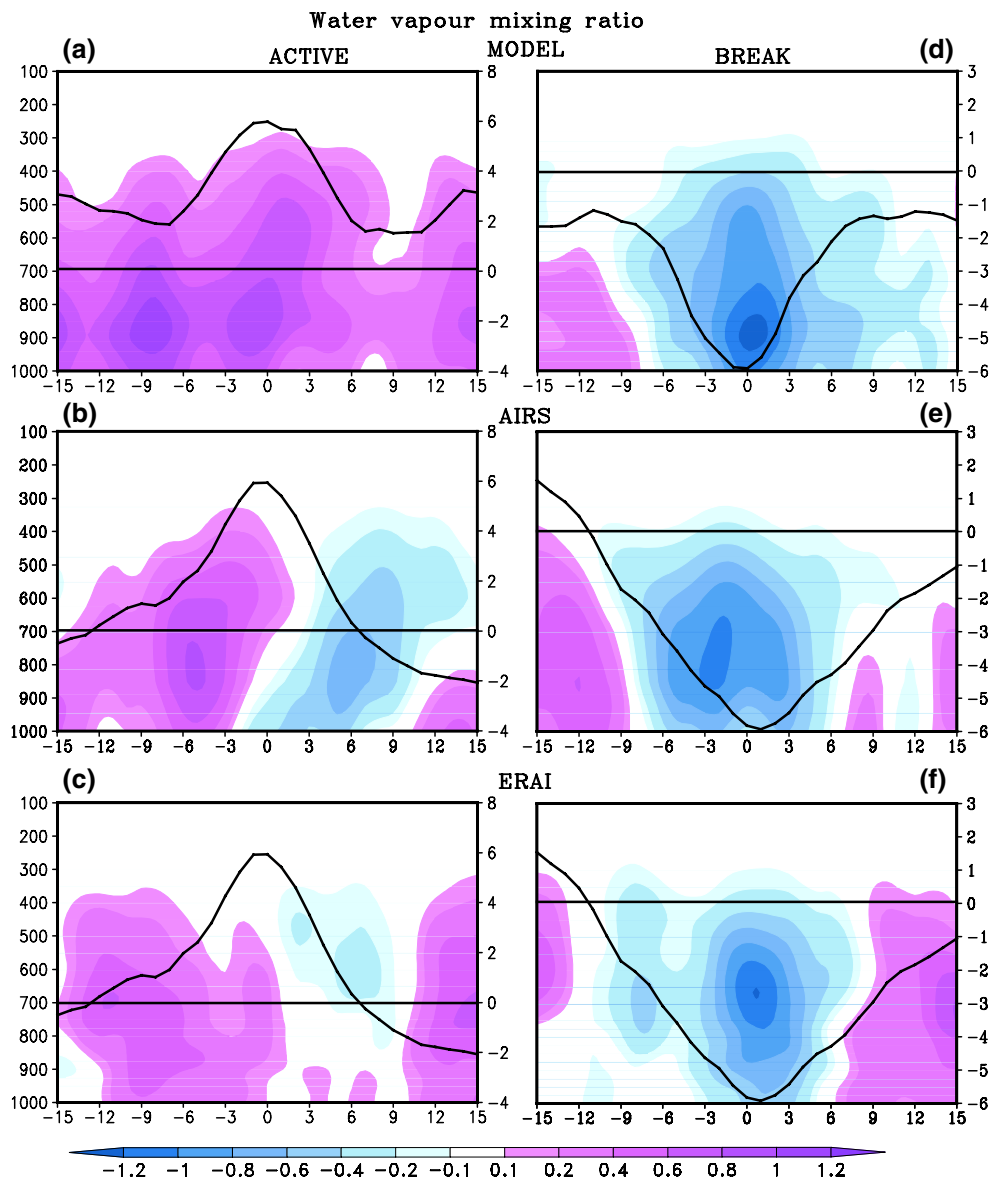
Fig. 12 The lead-lag evolution of composite WVMR anomalies (g Kg^{-1}) composite averaged over MCR for active (*left panels*) and break (*right panels*) phases from model (**a, d**), AIRS (**b, e**) and ERAI (**c, f**). The overlaid *solid line* represents rainfall anomalies (mm day^{-1}, scales at *right*)

strongly enhanced convection is generally preceded by a low-level moist anomaly and followed by a low-level dry anomaly in observations, which is not seen in the model. In contrast during the break phase, moisture anomalies are captured by the model and are in agreement with the observations.

Figure 13a, b shows the anomalous relative vorticity with height over the MCR during the active phase from model and ERAI respectively. Vorticity (Fig. 13b) from ERAI shows strong cyclonic circulation extending up to 200 hPa during the peak phase and the sharp fall in its magnitude by 2 pentads of active phase. The model failed to capture these features (Fig. 13a). During break (Fig. 13c),

the model has weak anticyclonic vorticity just prior to 1 pentad with double maxima (first one at 850 hPa and the second one at 450 hPa) and minima at 650 hPa. Another strong anticyclonic vorticity is evident after the 2 pentads which extent up to 100 hPa. In the case of ERAI (Fig. 13d) anticyclonic vorticity is reported during the peak phase of break and it remains up to the following two pentads and the first anticyclonic vorticity also has double peak with respect to height, first one at 900 hPa and second one at 200 hPa, which is one pentad ahead in the model. Thus model produced systematic evolution of vertical structure of vorticity over the MCR during the break phase compared to that of active phase. Overall model produces the spatial
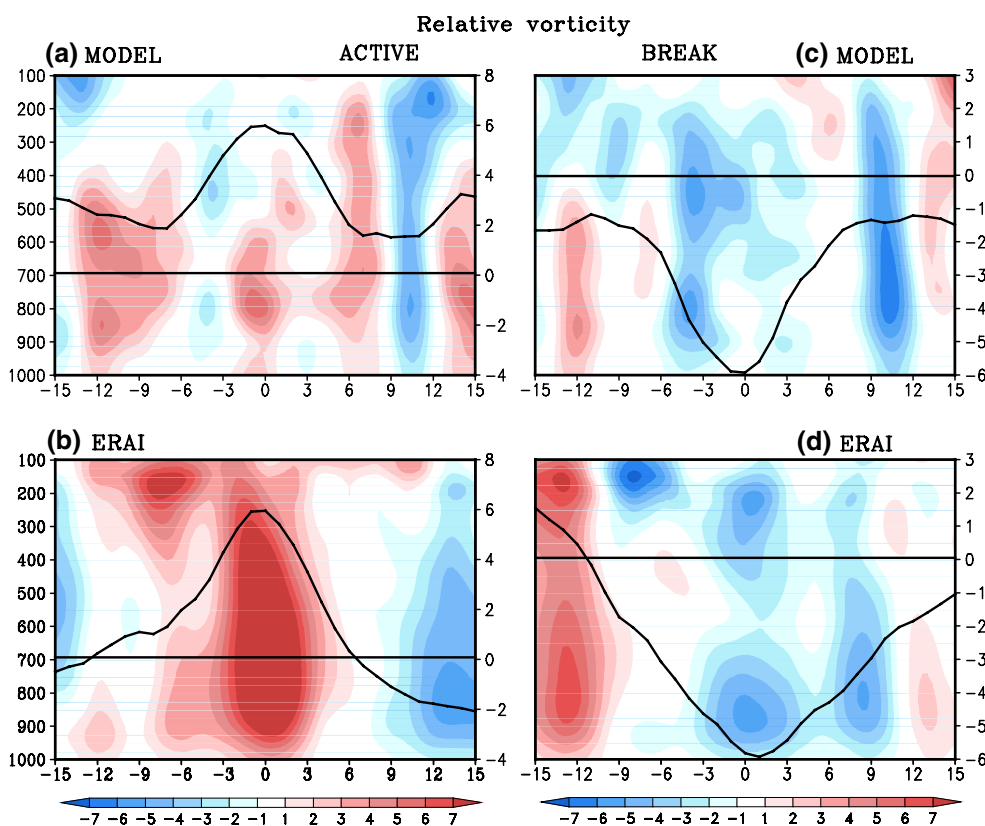
Fig. 13 The lead-lag evolution of composite relative vorticity anomalies ($\times 10^6$ s^{-1}) composite averaged over MCR for active (*left panels*) and break (*right panels*) phases from model (**a**, **c**) and ERAI (**b**, **d**). The overlaid *solid line* represents rainfall anomalies (mm day^{-1}, scales at *right*)

features of active and break phases like in observations, however vertical structure of temperature, WVMR and vorticity over the MCR during the active phase displays larger discrepancies than during the break period. This indicates the model inability in simulating high convective instability regimes.

6 Summary and discussion

RCMs have wide applications in the regional climate projections. Therefore the assessment of RCMs on the mean ISM features is very important. In this context, the present study quantifies the merits and demerits of the regional climate model (WRF) in simulating mean ISM. Model is forced by the NCEP FNL data for every year from 1 May to 1 October during 2001–2011. Temperature and WVMR profiles from AIRS, ERAI reanalysis and precipitation from IMD, GPCP and TRMM data are used for model assessment. The uniqueness of this study is that the chosen domain is large, and covers the entire monsoon region which allows the systematic evolution of the monsoon internal dynamics. The dynamic and moist thermodynamic processes associated with the seasonal mean and

intraseasonal features of ISM are systematically evaluated with the new generation of advanced satellite observations (AIRS) with special emphasis on their vertical structures. Our analysis reveals that large scale circulation and precipitation features of ISM are simulated by the model with some discrepancies. It is interesting to note that model could simulate some regional scale features such as heat low over north India, ridge line on the western parts of southern peninsular India, trough line off west coast of India, well-defined low level cyclonic circulation over the monsoon trough region, upper troposphere anticyclonic circulation and its position over the northeastern states of India, subtropical westerly jet and orographic precipitation.

The model could reproduce cross equatorial flow and LLJ but the core of LLJ is shifted southwestward in the model due to unrealistic convective heating over the lower latitudes of Indian Ocean and southern peninsular India. Strong easterly wind bias from the western Pacific to MCR and westerly wind bias in the western equatorial Indian Ocean are evident. These biases are due to unrealistic zonal pressure gradient around the equatorial region. The extent of TEJ is confined only up to 15°N, mainly due to the midtropospheric cold bias over the Tibetan region and weak wind shear. The model could simulate the convective

precipitation zones well, however the rainfall over ISM region is overestimated. The strong low level easterly wind bias from western Pacific and head BoB supports enhanced moisture transport towards MCR leading to strong WVMR in the lower to midtroposphere, resulting the overestimation of rainfall. Minimum RMSE and MAE is found over MCR while wet bias (RMSE (MAE) of 10 (8) mm day^{-1}) is noticed over Western Ghats and BoB. Unrealistic high precipitation is evident over the southwestern Indian Ocean in the model as in many GCMs. The northward migration of maximum rain band is limited to 23°N in the model (up to 28°N in observations), due to weaker vertical wind shear according to the thermal wind relation as a consequence of meridional asymmetric bias of SLP. The evolution of vertical structure of temperature has weaker baroclinic response associated with the precipitation compared to observations. The weak wind shear and overestimation of vorticity in the boundary layer are consistent with the strong convergence in the model. Thus seasonal mean monsoon features of the model are characterized by weak meridional pressure gradient, vertical wind shear and baroclinic response but strong convergence and WVMR loading result strong wet bias in the model. The evolution of vertical profiles of moist and thermodynamic structures indicates that strong lower-level convergence and upper level divergence associated with enhanced updrafts resulting from the strong moist unstable atmosphere. Further this may lead to moist biases in the precipitation which is consistent with the positive biases in the model over MCR.

The model has relatively more active and break events than observations. Large scale features associated with breaks are simulated relatively better than active phase in the model. During active phase, strong (weak) warm anomalies in the lower (mid) troposphere begin to increase at 3 pentads before the precipitation maximum in observations. This condition leads to unstable atmosphere by increasing CAPE and such a preconditioning in the lower troposphere is missed in the model. Overall, the model temperature anomalies over MCR exhibit bimodal vertical structure, that is, warm (cold) anomalies in the free troposphere and cold (warm) anomalies in the lower troposphere associated with enhanced (suppressed) convection. The model has critical bias in representing the gradual increase (decrease) of water vapor (temperature) in the boundary layer and its build up in the lower and midtroposphere ahead of peak intraseasonal rainfall. These biases might be related to the model mean vertical moist thermodynamic structures. These deficiencies can be improved with proper representation of vertical moist and thermodynamic structures in the model. This research has been taken up to produce model simulations at 45 km resolution to conform with CORDEX, and may differ when simulations are made at higher resolution. It is anticipated that these findings will significantly contribute to the regional climate model assessment programs such as CORDEX and the Regional Climate Model Intercomparison Project for Asia.

References

Anthes RA, Kuo YH, Hsie EY, Low-Nam S, Bettge TW (1989) Estimation of skill and uncertainty in regional numerical models. Q J R Meteorol Soc 115:763–806

Aumann HH, Chahine MT, Gautier C, Goldberg MD, Kalnay E, McMillin LM, Revercomb H, Rosenkranz PW, Smith WL, Staelin DH, Strow LL, Susskind J (2003) AIRS/AMSU/HSB on the Aqua mission: design, science objectives, data products, and processing systems. IEEE Trans Geosci Remote Sens 41(2):253–264

Betts AK, Miller MJ (1986) A new convective adjustment scheme. Part II: single column tests using GATE wave, BOMEX, and arctic air-mass data sets. Q J R Meteorol Soc 112:693–709

Bhaskar Rao DV, Ashok K, Yamagata T (2004) A numerical simulation study of the Indian summer monsoon of 1994 using NCAR MM5. J Meteorol Soc Jpn 82(6):1755–1777

Bhaskaran B, Jones RG, Murphy JM, Noguer M (1996) Simulations of the Indian summer monsoon using a nested climate model: domain size experiments. Clim Dyn 12:573–587

Bhaskaran B, Murphy JM, Jones RG (1998) Intraseasonal oscillation in the Indian summer monsoon simulated by global and nested regional climate models. Mon Weather Rev 126:3124–3134

Bhaskaran B, Ramachandran A, Jones R, Moufouma-Okia W (2012) Regional climate model applications on sub-regional scales over the Indian monsoon region: the role of domain size on downscaling uncertainty. J Geophys Res 117:D10113. doi:10.1029/2012JD017956

Boos WR, Hurley JV (2013) Thermodynamic bias in the multi-model mean boreal summer monsoon. J Clim 26:2279–2287

Chen SH, Sun WY (2002) A one dimensional time-dependent cloud model. J Meteorol Soc Jpn 80:99–118

Choudhury AD, Krishnan R (2011) Dynamical response of the South Asian monsoon trough to latent heating from stratiform and convective precipitation. J Atmos Sci 68:1347–1363

Diaconescu EP, Laprise R (2013) Can add be expected in RCM-simulated large scales? Clim Dyn 40:1769. doi:10.1007/s00382-012-1649-9

Divakarla MG, Barnet CD, Goldberg MD, McMillin LM, Maddy E, Wolf W, Zhou L, Liu X (2006) Validation of Atmospheric Infrared Sounder temperature and water vapor retrievals with matched radiosonde measurements and forecasts. J Geophys Res 111:D09S15. doi:10.1029/2005JD006116

Dobler A, Ahrens B (2010) Analysis of the Indian summer monsoon system in the regional climate model COSMO-CLM. J Geophys Res 115:D16101

Dudhia J (1989) Numerical study of convection observed during the winter monsoon experiment using a mesoscale two-dimensional model. J Atmos Sci 46:3077–3107

Feng J, Fu C (2006) Inter-comparison of 10-year precipitation simulated by several RCMs for Asia. Adv Atmos Sci 23:531–542

Fu XH, Wang B, Tao L (2006) Satellite data reveal the 3-D moisture structure of tropical intraseasonal oscillation and its coupling with underlying ocean. Geophys Res Lett 33:L03705. doi:10.1029/2005GL025074

Gadgil S (1996) Climate change and agriculture-An Indian perspective. In: Abool YR, Gadgil S, Pant GB (eds) Climate variability and agriculture. Narosa, New Delhi, pp 1–18

Goswami BN (2005) South Asian monsoon. In: Lau WKM, Waliser DE (eds) Intraseasonal variability of the atmosphere–ocean climate system, Chap. 2. Springer, Berlin, pp 19–61

Goswami BN, Ajayamohan RS, Xavier PK, Sengupta D (2003) Clustering of synoptic activity by Indian summer monsoon intraseasonal oscillations. Geophys Res Lett 30(8):1431. doi:10.1029/2002GL016734

Goswami BN, Venugopal V, Sengupta D, Madhusoodanan MS, Xavier PK (2006) Increasing trend of Extreme Rain Events over India in a Warming Environment. Science 314:1442–1445

Goswami BB, Mani NJ, Mukhopadhyay P, Waliser DE, Benedict JJ, Maloney ED, Khairoutdinov M, Goswami BN (2011) Monsoon intraseasonal oscillations as simulated by the superparameterized Community Atmosphere Model. J Geophys Res 116:D22104. doi:10.1029/2011JD015948

Hariprasad D, Venkata Srinivas C, Venkata Bhaskar Rao D, Anjaneyulu Y (2011) Simulation of Indian monsoon extreme rainfall events during the decadal period 2000–2009 using a high resolution mesoscale model. Adv Geosci A6:31–48

Holton JR (2004) An introduction to dynamical meteorology, 4th edn. Acadamic Presss, New York

Huffman GJ, Adler RF, Morrissey M, Bolvin DT, Curtis S, Joyce R, McGavock B, Susskind J (2001) Global precipitation at one-degree daily resolution from multi-satellite observations. J Hydrometeorol 2:36–50. doi:10.1175/1525-7541(2001)002<0036:GPAODD>2.0.CO;2

Huffman GJ, Adler RF, Bolvin DT, Gu G, Nelkin EJ, Bowman KP, Hong Y, Stocker EF, Wolff DB (2007) The TRMM multisatellite precipitation analysis (TMPA): quasi-global, multiyear, combined-sensor precipitation estimates at fine scales. J Hydrometeorol 8:38–55

Jacob D, Podzum R (1997) Sensitivity studies with the Regional Climate Model REMO. Meteorol Atmos Phys 63:119–129

Janjic ZI (1994) The step-mountain eta coordinate model. Further developments of the convection, viscous sublayer and turbulence closure schemes. Mon Weather Rev 122:927–945

Jiang X, Li T, Wang B (2004) Structures and mechanisms of the northward propagating boreal summer intraseasonal oscillation. J Clim 17:1022–1039

John VO, Soden BJ (2007) Temperature and humidity biases in global climate models and their impact on climate feedbacks. Geophys Res Lett 34:L18704. doi:10.1029/2007GL030429

Joseph PV, Sijikumar S (2004) Intraseasonal variability of the low-level jet stream of the Asian summer monsoon. J Clim 17:1449–1458

Kripalani RH, Oh JH, Kulkarni A, Sabade SS, Chaudhari HS (2007) South Asian summer monsoon precipitation variability: coupled climate model simulations and projections under IPCC AR4. Theor Appl Climatol 90(3–4):133–159. doi:10.1007/s00704-006-0282-0

Krishna Kumar K, Hoerling M, Rajagopalan B (2005) Advancing dynamical prediction of Indian monsoon rainfall. Geophys Res Lett 32(8):L08704. doi:10.1029/2004GL021979,4

Krishnamurthy V, Shukla J (2000) Intra-seasonal and inter-annual variability of rainfall over India. J Clim 13:4366–4377

Krishnamurti TN, Bhalme HN (1976) Oscillations of a monsoon system, Part I: observational aspects. J Atmos Sci 33:1937–1954

Lee DK, Suh MS (2000) Ten year East Asian summer monsoon simulation using a regional climate model (RegCM2). J Geophys Res 105:29565–29577

Lucas-Picher P, Christensen JH, Saeed F, Kumar P, Asharaf S, Ahrens B, Wiltshire A, Jacob D, Hagemann S (2011) Can regional climate models represent the Indian monsoon? J Hydrometeorl. doi:10.1175/2011JHM1327.1mm

Meehl GA (1994) Coupled ocean-atmosphere-land processes and South Asian monsoon variability. Science 265:263–267

Mlawer EJ, Taubman SJ, Brown PD, Iacono MJ, Clough SA (1997) Radiative transfer for inhomogeneous atmosphere: RRTM, a validated correlated-k model for the long-wave. J Geophys Res 102(D14):16663–16682

Monin AS, Obukhov AM (1954) Basic laws of turbulent mixing in the surface layer of the atmosphere (in Russian). Contrib Geophys Inst Acad Sci USSR 151:163–187

Mooley DA, Parthasarathy B (1984) Fluctuations in all-india summer monsoon rainfall during 1871-1978. Clim Change 6:287–301

Mukhopadhyay P, Taraphdar S, Goswami BN, Krishna Kumar K (2010) Indian summer monsoon precipitation climatology in a high resolution regional climate model: impact of convective parameterization on systematic biases. Wea Forecast 25:369–387

Nie J, Boos W, Kuang Z (2010) Observational evaluation of a convective quasi-equilibrium view of monsoons. J Clim 23:4416–4428

Noh Y, CheonWG Hong S-Y, Raasch S (2003) Improvement of the K-profile model for the planetary boundary layer based on large eddy simulation data. Bound Layer Meteor 107:401–427

Parkinson CL (2003) Aqua: an Earth-Observing Satellite mission to examine water and other climate variables. IEEE Trans Geosci Remote Sens 41:173–183

Rajeevan M, Bhate J, Kale JD, Lal B (2006) High resolution daily gridded rainfall data for the Indian region: analysis of break and active monsoon spells. Curr Sci 91:293–306

Rajeevan M, Gadgil S, Bhate J (2010) Active and break spells of the Indian summer monsoon. J Earth Syst Sci 119(3):229–247

Rajeevan M, Rohini P, Niranjan Kumar K, Srinivasan J, Unnikrishnan CK (2013) A study of vertical cloud structure of the Indian summer monsoon using CloudSat data. Clim Dyn 40:637–650

Raju A, Parekh A, Gnanaseelan C (2014a) Evolution of vertical moist thermodynamic structure associated with the Indian summer monsoon in a regional climate model. Pure Appl Geophys. 171:1499–1518 doi:10.1007/s00024-013-0697-3

Raju A, Parekh A, Chowdary JS, Gnanseelan C (2014b) Impact of satellite retrieved atmospheric temperature profiles assimilation on Asian summer monsoon simulation. Theor Appl Climatol 116:317–326

Ramage CS (1971) Monsoon meteorology. Academic Press, New York

Ratnam JV, Giorgi F, Kaginalkar A, Cozzini S (2009) Simulation of the Indian monsoon using the RegCM3–ROMS regional coupled model. Clim Dyn. doi:10.1007/s00382-008-0433-3

Saeed F, Hagemann S, Jacob D (2012) A framework for the evaluation of the South Asian summer monsoon in a regional climate model applied to REMO. Int J Climatol 32:430–440. doi:10.1002/joc.2285

Schaefer JT (1990) The critical success index as an indicator of forecasting skill. Weather Forecast 5:570–575

Simmons A, Uppala S, Dee D, Kobayashi S (2007) ERA-Interim: New ECMWF reanalysis products from 1989 on-wards. ECMWF Newsletter, No. 110, ECMWF, Reading, UK, pp 25–35

Skamarock WC, Klemp J, Dudhia J, Gill DO, Barker DM, Wang W, Powers JG (2008) A description of the advanced research WRF version 2. NCAR technical note, NCAR/TN-468 + STR. Mesoscale and Microscale Meteorology Division, National Center for Atmospheric Research, Boulder, CO, USA

Srinivas CV, Hariprasad D, Bhaskar Rao DV, Anjaneyulu Y, Baskarana R, Venkataramana B (2012) Simulation of the Indian

summer monsoon regional climate using advanced research WRF model. Int J Climatol. doi:10.1002/joc.3505

Taraphdar S, Mukhopadhyay P, Goswami BN (2010) Predictability of Indian summer monsoon weather during active and break phases using a high resolution regional model. Geophys Res Lett 37:L21812. doi:10.1029/2010GL044969

Thiebaux J, Rogers E, Wang W, Katz B (2003) A new high resolution blended real-time global sea surface temperature analysis. Bull Am Meteorol Soc 84:45–656

Tian B, Waliser DE, Fetzer EJ, Yung YL (2010) Vertical moist thermodynamicstructure of the Madden–Julian Oscillation in Atmospheric Infrared Sounder observations: an update and a comparison to ECMWF interim reanalysis. Mon Weather Rev 138:4576–4882

Vernekar AD, Ji Y (1999) Simulation of the onset and intraseasonal variability of two contrasting summer monsoons. J Clim 12:1707–1725

Waliser DE et al (2003) AGCM simulations of intraseasonal variability associated with the Asian summer monsoon. Clim Dyn 21:423–446. doi:10.1007/s00382-003-0337-1

Wang Y, Leung LR, McGregor JL, Lee DK, Wang WC, Ding Y, Kimura F (2004) Regional climate modeling: progress, challenges and prospects. J Meteorol Soc Jpn 82(6):1599–1628

Webster PJ, Palmer T, Yanai M, Tomas R, Magana V, Shukla J, Yasunari A (1998) Monsoons: processes, predictability and the prospects for prediction. J Geophys Res 103:14451–14510

Wong S, Fetzer EJ, Tian B, Lambrigtsen B (2011) The apparent water vapor sinks and heat sources associated with the intraseasonal oscillation of the Indian summer monsoon. J Clim 24:4466–4479

Wu G, Liu Y, He B, Bao Q, Duan A, Fei-Fei J (2012) Thermal Controls on the Asian Summer. Monsoon Sci Rep 2:404. doi:10.1038/srep00404